Degenerate perturbation theory of quantum fluctuations in a pyrochlore antiferromagnet

Doron L. Bergman,[1] Ryuichi Shindou,[1] Gregory A. Fiete,[2] and Leon Balents[1]
[1]*Department of Physics, University of California, Santa Barbara, California 93106-9530, USA*
[2]*Kavli Institute for Theoretical Physics, University of California, Santa Barbara, California 93106-4030, USA*
(Received 1 September 2006; revised manuscript received 5 January 2007; published 2 March 2007)

We study the effect of quantum fluctuations on the half-polarized magnetization plateau of a pyrochlore antiferromagnet. We argue that an expansion around the easy-axis limit is appropriate for discussing the ground-state selection among the classically degenerate manifold of collinear states with a 3:1 ratio of spins parallel and/or antiparallel to the magnetization axis. A general approach to the necessary degenerate perturbation theory is presented, and an effective quantum dimer model within this degenerate manifold is derived for arbitrary spin s. We also generalize the existing semiclassical analysis of Hizi and Henley [Phys. Rev. B **73**, 054403 (2006)] to the easy-axis limit and show that both approaches agree at large s. We show that under rather general conditions, the first nonconstant terms in the effective Hamiltonian for $s \geqslant 1$ occur only at sixth order in the transverse exchange coupling. For $s \geqslant 5/2$, the dominant terms in the effective Hamiltonian are those of a *classical* dimer model, which predicts a magnetically ordered state. For $s \leqslant 2$, more exotic possibilities may be realized. The effective dimer Hamiltonian is then strongly quantum. We describe two likely ground states in that regime.

DOI: 10.1103/PhysRevB.75.094403 PACS number(s): 75.10.Jm, 75.25.+z

I. INTRODUCTION

Magnetism is an inherently quantum-mechanical effect that ultimately arises from the exchange processes in an interacting many-particle quantum system. Thus, magnetic systems can reveal much about the richness of quantum mechanics itself, especially when cooperative effects are operational and emergent effective low-energy theories describe the relevant physics. A few notable theoretical examples are the spin-liquid phases obtained in frustrated magnets.[1–5] Quantum effects may play a central role in other types of order as well. Recent experiments on a number of insulating chromate compounds, namely, $CdCr_2O_4$ and $HgCr_2O_4$, have shown peculiar features in the low-temperature magnetization as a function of applied magnetic field. At low temperatures, the magnetization grows linearly with magnetic field up to some critical value at which point there is a sharp jump in magnetization onto a rather wide plateau with half the full saturation magnetization.[6–8] With sufficiently large fields, it is possible to observe a smooth transition off the half-magnetization plateau and a gradual increase in magnetization up to what may be a fully polarized plateau state.[6] As described in Ref. 9, it is expected that the magnetism in these compounds is well described by the Heisenberg antiferromagnet (AFM) of spin $s=\frac{3}{2}$ on the pyrochlore lattice.

Motivated by these experimental examples of a half polarization plateau in the pyrochlore Heisenberg AFM, we conduct a theoretical study of the quantum pyrochlore Heisenberg AFM for any spin value s in a strong magnetic field focusing on a half polarization plateau. While the physics of $HgCr_2O_4$ is probably determined to a large degree by the classical physics of spin-lattice interactions,[10–14] it may be that in other similar compounds where coupling to phonons is weak, quantum effects could play a significant role.

In any case, the general problem of determining the spin state on plateaus of nonzero magnetization in frustrated magnets occurs in a large number of materials.[15–22] At fields large enough to induce substantial magnetization, the ground state is expected to be very different from the zero-field state, and one would ideally pursue a theoretical approach that takes advantage of the large external field. The methods developed indeed use this explicitly, and the particular application to the half-polarized pyrochlore magnetization plateau provides a rather nontrivial test bed. We make use of the large field to justify an easy-axis approximation to a nearest-neighbor *XXZ* antiferromagnetic in an external field. Physically, at large fields, the spin is oriented on average more along the field axis than transverse to it. Furthermore, specifically on a magnetization plateau, general arguments imply that the static transverse moment vanishes *on every site*, $\langle S_i^{\pm} \rangle = 0$. Thus, we expect that degenerate perturbation theory (DPT) about the easy-axis (Ising) limit should be justified on the plateau, and one may thereby derive an effective Hamiltonian. This effective Hamiltonian acts in the *constrained* "3:1" space of states with three majority spins with $S_i^z = +s$ and one minority spin with $S_i^z = -s$ on each tetrahedron. This space is macroscopically degenerate, and all its members have half the saturation magnetization.

The reader may well wonder whether there is any need for an approach of this sort, given the successes of the large-s semiclassical spin-wave method in many other contexts. Indeed, for unfrustrated antiferromagnets, it is known that the $1/s$ expansion gives reasonably convergent results even down to $s=1/2$. However, this convergence is strongly dependent upon the lattice—large corrections to the spin-wave dispersion have recently been obtained even for the rather weakly frustrated triangular lattice.[23,24] In highly frustrated magnets such as the pyrochlore, another approach is warranted. Particularly worrisome in the $1/s$ expansion is the difficulty of treating *tunneling*, which is nonperturbative in this method.[25–27] By contrast, in the easy-axis expansion, tunneling and virtual exchange are treated on the same footing. Of course, for large s, both approaches must agree, and

we will indeed check that this is the case in our specific application.

The effective Hamiltonian describing splittings within the degenerate manifold of Ising ground states will generally take the form of a constrained quantum Ising model. As explained in a previous publication,[9] for the case of the pyrochlore half-magnetization plateau in the easy-axis limit, it can be cast in the form of a "quantum dimer model" (QDM) on the bipartite diamond lattice. Such QDMs are known to display both ordered and disordered (spin-liquid) ground states in different regions of their phase diagrams.[2,4,28–31] We derive the parameters of this QDM for general s and discuss several limits and the expectations for the plateau ground state. For simplicity of presentation, we perform this calculation here for the simplest *XXZ* spin model with no additional anisotropy or other spin interaction terms. However, the method is straightforwardly generalized to include other on-site (e.g., uniaxial anisotropy[32]) or nearest-neighbor (e.g., biquadratic) interactions without substantial increase in computational complexity. More generally, the flexibility to include such effects allows one to consider the quantum effects upon the ground-state selection within a magnetization plateau even when the dominant mechanism of plateau *stabilization* is a classical one.

A remarkable feature of the DPT is that all diagonal terms describing splitting of the low-energy manifold *vanish below sixth order.* For $s \geqslant 1$, off-diagonal tunneling terms also vanish up to this order, so that the entire effective Hamiltonian is determined by terms of sixth order and higher. This behavior is similar to a result of Hizi and Henley[26] that in the large-s limit, the effective Hamiltonian is expressed entirely in terms of a "spin flux" variable involving a product of six spins around an elementary loop of the lattice. We show here that our result is rather general and originates from two basic features: the absence of nontrivial loops of length less than six links on the pyrochlore lattice and the fact that all low-energy spin states on a single tetrahedron are permutations of one another. From our proof of this result, it can be readily seen that similar behavior holds for any lattice of corner sharing simplexes with only on-site and nearest-neighbor interactions and permutation-related ground states on a single simplex. We will apply the methods of this paper to other such problems of interest in future work.

For the pyrochlore magnetization plateau and QDM studied here, the conclusions are as follows. For $s \geqslant 3$, we find that *diagonal* terms in the QDM are much larger than off-diagonal ones. In this case, the latter are negligible, and because the diagonal QDM is effectively classical, it is soluble and the ground state is *ordered*. We discuss the preferred spin ordered states as a function of s. For $s \leqslant 5/2$, the off-diagonal terms are non-negligible, and a simple solution is no longer available. For $s \leqslant 3/2$, the off-diagonal term in the QDM is dominant. In this case, we expect one of two possible likely states. One is a state adiabatically connected to (and possessing the same symmetries as) the **R** state discussed previously in Ref. 9, which is the state containing the maximal number of hexagonal loops with alternating spins (flippable plaquettes in the QDM language). Another likely state is the U(1) spin liquid. Indeed, as argued in Ref. 33, it is quite possible that the simplest QDM displays a direct quantum phase transition between these two states. For $s = 2, 5/2$, the diagonal and off-diagonal terms are comparable. Various arguments lead us to still expect the same two candidate states as for $s \leqslant 3/2$, perhaps with a *better* chance of a U(1) spin liquid than for $s \leqslant 3/2$. A definite conclusion for $s \leqslant 5/2$ must await more serious computational (e.g., quantum Monte Carlo) analysis.

The ground state of the QDM just discussed is determined only by the *dimensionless* ratios of coupling constants. However, the DPT calculation also gives the overall scale of the effective interaction in terms of the microscopic exchange J. For $s=3/2$ (relevant to $HgCr_2O_4$), the largest energy scale (extrapolated from the easy-axis perturbation theory to the Heisenberg limit) generated by quantum fluctuations is that of the off-diagonal term and ≈ 0.25 J. Were this the true scale for ground-state selection in the degenerate 3:1 manifold in $HgCr_2O_4$, the magnetic ordering would occur at a temperature of this order, i.e., ≈ 2.5 K. Experimentally, magnetic ordering is observed at a substantial fraction of the temperature of onset of the plateau formation, which is around 6 K. It is therefore plausible that quantum fluctuations may be driving the ordering observed in $HgCr_2O_4$. However, it is equally plausible that the ordering is determined by other mechanisms. The closeness of the ordering and plateau scales in experiment suggests that both are determined by the *same* physical mechanism. Indeed, we have recently shown[10] that the same spin-lattice coupling which leads to plateau formation can also account for the state selection. Curiously, the **R** state is also stabilized by the lattice mechanism. This is symptomatic of the very strong constraints defining the 3:1 QDM states, which lead rather different microscopic interactions to favor the same ground state. For $s=1$ and $s=1/2$, the DPT gives much larger characteristic scales for the QDM, the off-diagonal term being of orders of 0.88 and 1.5 J in the two cases. Thus, such $s \leqslant 1$ antiferromagnets, if realized experimentally, would be even more promising systems to observe quantum fluctuation effects.

This paper is organized as follows. In Sec. II, we describe our theoretical model, the nearest-neighbor quantum Heisenberg antiferromagnet on a pyrochlore lattice in an external field. An easy-axis limit is taken under the assumption of the suppression of transverse spin fluctuations in large magnetic fields. After applying degenerate perturbation theory (DPT) in the transverse spin fluctuations, an effective dimer model that can be used to obtain an approximate ground state of the original model emerges in Sec. III. In Sec. IV, we carry out a large-s analysis of the *XXZ* model, deriving a different effective Hamiltonian splitting the 3:1 manifold of degenerate states. This effective Hamiltonian turns out to coincide with the $s \to \infty$ limit of the effective Hamiltonian from the DPT analysis. In Sec. V, we explore the ground state of the diagonal part of the effective Hamiltonian from DPT. In Sec. V B, we explore in more generality the appropriate quantum dimer model (QDM) of which all our effective Hamiltonians are special cases. We conclude the main text of this paper with a discussion of our results in Sec. VI. In Appendix A, we analyze how the half polarization plateau is modified by quantum fluctuations. An alternative method of performing DPT is presented in Appendix B and shows perfect agree-

ment with the result of Sec. III. Finally, in Appendix C, we explore the states degenerate with the $\sqrt{3}\times\sqrt{3}$ states found for $s=\frac{3}{2}$.

II. MODELS

A. Hamiltonians and limits

We begin with the simple spin-s Heisenberg antiferromagnet (AFM) residing on the sites of the pyrochlore lattice in the presence of a magnetic field $\mathbf{H}$,

$$\mathcal{H}=J\sum_{\langle ij\rangle}\mathbf{S}_i\cdot\mathbf{S}_j-\mathbf{H}\cdot\sum_j\mathbf{S}_j. \tag{1}$$

On the pyrochlore lattice, one may recast the nearest-neighbor exchange in terms of the total spin on tetrahedra using the identity

$$2\sum_{\langle ij\rangle}\mathbf{S}_i\cdot\mathbf{S}_j=\sum_t(\mathbf{S}_t)^2-\sum_t\sum_{j\in t}(\mathbf{S}_j)^2, \tag{2}$$

where $\mathbf{S}_t=\Sigma_{j\in t}\mathbf{S}_j$ is the sum of spins on a tetrahedron labeled by t, and $(\mathbf{S}_j)^2|j\rangle=S(S+1)|j\rangle$. This gives the more convenient form

$$\mathcal{H}=\frac{J}{2}\sum_t[(\mathbf{S}_t-\mathbf{h})^2-\mathbf{h}^2], \tag{3}$$

where we have introduced the dimensionless magnetic field $\mathbf{h}=\mathbf{H}/2J=h\hat{z}$ and ignored a trivial constant term in the Hamiltonian.

1. Classical limit

The form in Eq. (3) makes the behavior in the large-s limit apparent. In this limit, the spins behave classically, and one may replace $\mathbf{S}_i\to s\hat{n}_i$, where $\hat{n}_i$ is a unit vector. The ground states then consist simply of all states for which $\mathbf{S}_t=s\Sigma_{i\in t}\hat{n}_i=\mathbf{h}$ on every tetrahedron. This set has a large continuous degeneracy. Furthermore, since the magnetization is simply half the sum of the $\mathbf{S}_t$ (because each spin is contained in two tetrahedra), this implies a continuous linear behavior of the magnetization with field. Thus, in this model, magnetization plateaus can emerge only from quantum corrections to the classical limit.

2. Easy-axis limit

An alternative approach exploits the fact that, with the application of the magnetic field, the global SU(2) symmetry of the bare Heisenberg model is broken down to a U(1) symmetry (rotations about the magnetic-field direction). Moreover, when the magnetization per spin is substantial, on average the transverse components $S_i^{\pm}$ are smaller in magnitude than the longitudinal ones. It is therefore natural to treat transverse and longitudinal exchange couplings on a different footing, with the latter taking the dominant role. Formally, this is accomplished by replacing the isotropic Heisenberg Hamiltonian by an XXZ model:

$$\mathcal{H}=\mathcal{H}_0+\mathcal{H}_1, \tag{4}$$

where

$$\mathcal{H}_0=\frac{J_z}{2}\sum_t[(S_t^z-h)^2-h^2]-J_z\sum_i(S_i^z)^2 \tag{5}$$

and

$$\mathcal{H}_1=\frac{J_\perp}{2}\sum_{\langle ij\rangle}(S_i^+S_j^-+\text{H.c.}). \tag{6}$$

We use the notation $S_t^z=\Sigma_{i\in t}S_i^z$, and we have made use of the identity

$$\sum_{\langle ij\rangle}S_i^zS_j^z=\frac{1}{2}\sum_t(S_t^z)^2-\sum_i(S_i^z)^2. \tag{7}$$

In the equations above, and elsewhere in this paper, $\langle ij\rangle$ denotes a sum over nearest-neighbor sites on the pyrochlore lattice and $S_i^{\pm}$ are the spin ladder operators. Note that in the Heisenberg model $J_\perp=J_z=J$, but the more general XXZ model has all the same symmetries as the former even when this condition is not obeyed. From the above reasoning, we expect that the transverse terms involving $J_\perp$ may be treated as "small" perturbations in the strong-field regime of interest. We note that this is expected to be a particularly good approximation when the system exhibits a magnetization plateau. This is because, as described in the Introduction, $\langle S_i^{\pm}\rangle$ must vanish in such a state. Formally, this "easy-axis" limit consists of taking $J_\perp\ll J_z$ and doing degenerate perturbation theory in $\alpha=J_\perp/J_z$. We will assess the validity of this approximation later by considering the *magnitude* of the perturbative corrections extrapolated to $\alpha=1$. Finally, we note that several other effects can stabilize a collinear state. One is the addition of easy-axis anisotropy,

$$\mathcal{H}_0'=-K\sum_i(S_i^z)^2, \tag{8}$$

with $K\gg J_\perp>0$. A second mechanism is biquadratic exchange,

$$\mathcal{H}_0''=-bJ\sum_{\langle ij\rangle}(\mathbf{S}_i\cdot\mathbf{S}_j)^2, \tag{9}$$

with $b>0$. A term of this form can be generated dynamically from spin-lattice interactions, known to be strong in $HgCr_2O_4$. The DPT treatment discussed below can readily be generalized to include either or both of the terms in Eqs. (8) and (9). For simplicity of presentation, we do not do so here. While easy-axis terms similar to Eq. (8) are allowed for $s>1/2$, this particular simple form, with the same spatial direction for the local easy axis of all spins, is not physically appropriate for the cubic pyrochlore spinels, and the proper anisotropy terms allowed by symmetry in these materials are likely to be very small in any case.

B. Magnetization process in the Ising model

The evolution of the ground state with field in the extreme easy-axis limit $\alpha=0$ is less trivial than in the classical limit. The system is then described by the Ising Hamiltonian, Eq. (5). We shall focus on the $h\geqslant 0$ case, as the case $h\leqslant 0$ is equivalent. The expression Eq. (5) can be written as a sum over tetrahedra $\mathcal{H}_0=\Sigma_t\mathcal{H}_t$ with

$$\mathcal{H}_t = \frac{J_z}{2}\left[(S_t^z - h)^2 - h^2 - \sum_{j\in t}(S_j^z)^2\right], \tag{10}$$

and therefore if one can minimize this energy on each single tetrahedron, one will have attained the minimum energy of the many-body system.

The magnetization S_t^z of any individual tetrahedron is *quantized* to the values $S_t^z = 0, \pm 1, \pm 2, \ldots, \pm 4s$. The first term in Eq. (10) favors the magnetization of the tetrahedron to take on a value close to the integer part of the dimensionless magnetic field. The second term in Eq. (10) favors larger z components of the spin values $S_j^z = \pm s$. This second term is trivial only in the spin $\frac{1}{2}$ case where the spin $\frac{1}{2}$ Pauli matrices square to the identity.

A state with the magnetization $S_t^z = m = [h]$ (the integer part of h) clearly minimizes the energy of the first term in Eq. (10). However, given the magnetization, there is some freedom for the values of the spins on each tetrahedron. The second term in Eq. (10) reduces this freedom by adding an energy cost for small S^z components.

Consider four spins on a tetrahedron with total magnetization m and individual values of S_1^z, S_2^z, S_3^z, and S_4^z. Now, compare the energy of this state with that of $S_1^z - 1$, $S_2^z + 1$, S_3^z, and S_4^z. The only energy difference comes from the third term in Eq. (10),

$$\Delta E = -(S_1^z + 1)^2 - (S_2^z - 1)^2 + (S_1^z)^2 + (S_2^z)^2 = -2(1 - S_1^z + S_2^z). \tag{11}$$

From this expression, one deduces that if one begins with $S_2^z > S_1^z$, then it is energetically favorable to increase S_2^z even more at the expense of S_1^z. This increase in S_2^z can only be halted by one of $S_{1,2}^z$ reaching an *extreme* spin value of $\pm s$. From this reasoning, we conclude that the lowest-energy state on a single tetrahedron with a fixed total magnetization m has a spin configuration with the largest possible number of extreme valued spins. This also makes intuitive sense, since ideally *all* the spins should take on extreme values if possible. In three particular choices of m, all the spins take on extreme values: zero magnetization $m=0$ with s, s, $-s$, and $-s$; half polarization of $m=2s$ with s, $-s$, $-s$, and $-s$; and full polarization $m=4s$ with s, s, s, and s. For $m<2s$, we find the lowest-energy configuration for the spins s, s, $-s$, and $m-s$, and for $m>2s$, we find s, s, s, and $m-3s$. Finally, we can find the minimal energy for given magnetization m by using the spin configurations described above for every value of m and plugging them into Eq. (10). For $m<2s$, we find

$$E_m = \frac{J_z}{2}[2m(s-h) - 4s^2], \tag{12}$$

and for $m>2s$, we find

$$E_m = \frac{J_z}{2}[2(m-2s)(3s-h) - 4hs]. \tag{13}$$

From the above expressions, it is easy to see that at $h=s$, all $m<2s$ yield the same energy—all these states are degenerate at this field value. Similarly, for $h=3s$, all $m>2s$ yield the same energy. For other values of the magnetic field, we find for $h<s$ the lowest-energy state is the $m=0$ zero magnetization state; for $h<s<3s$, the lowest-energy state is the $m=2s$ half-polarized state; and for $h>3s$, the lowest-energy state is the $m=4s$ fully polarized state.

The three lowest-energy states in the various magnetic-field ranges have all spins at extreme values $\pm s$ and can be realized on every tetrahedron in the pyrochlore lattice. The $m=0$ state induces a degenerate manifold of states with every tetrahedron having s, s, $-s$, and $-s$ on it. This 2:2 proportionality is well known as the "ice rules" encountered in a particular phase of water ice,[34] as well as spin ice compounds.[35] The half-polarization states are also massively degenerate, with every tetrahedron in a 3:1 proportionality of $S_j^z = +s$ to $S_j^z = -s$ spins (or 3 up, 1 down). This particular degenerate manifold will be the focus of the remainder of our discussion. To summarize, the magnetization curve for Eq. (5) exhibits three plateaus at zero, half, and full polarizations for all values of s.

III. EASY-AXIS DEGENERATE PERTURBATION THEORY

A. Structure of perturbation theory

1. Basic formulation

In the previous section, we observed that the extreme easy-axis limit of the Heisenberg model exhibits a broad magnetization plateau at half-polarization. However, the ground states on this plateau are macroscopically degenerate, consisting of all states with a 3:1 ratio of majority and minority spins on each tetrahedron. In this section, we study the splitting of this degeneracy by perturbation theory in $J_\perp$. We employ the following formulation of degenerate perturbation theory (DPT). Define the projection operator $\mathcal{P}$ onto any degenerate manifold of states M. Consider any exact eigenstate $|\Psi\rangle$. Its projection $|\Psi_0\rangle = \mathcal{P}|\Psi|$ satisfies the "effective Schrödinger equation"

$$\left[E_0 + \mathcal{P}\mathcal{H}_1 \sum_{n=0}^{\infty} \mathcal{G}^n \mathcal{P}\right]|\Psi_0\rangle = E|\Psi_0\rangle = \mathcal{H}_{\text{eff}}|\Psi_0\rangle, \tag{14}$$

where the operator $\mathcal{G} = [1/(E - \mathcal{H}_0)](1 - \mathcal{P})\mathcal{H}_1$. Because the resolvent contains the exact energy E, Eq. (14) is actually a nonlinear eigenvalue problem. However, to any given order of DPT, E may be expanded in a series in $J_\perp$ to obtain an equation with a true Hamiltonian form within the degenerate manifold. Each factor of $\mathcal{G}$ is at least of $O(J_\perp)$ due to the explicit factor in $\mathcal{H}_1$, with higher-order corrections coming from the expansion of E. Once $|\Psi_0\rangle$ and E are known, the full wave function can be reconstructed as $|\Psi\rangle = (1 - \mathcal{G})^{-1}|\Psi_0\rangle = \Sigma_{n=0}^{\infty}\mathcal{G}^n|\Psi_0\rangle$.

Considering the lowest-order term in DPT that breaks the degeneracy, the precise energy $E = E_0 + O(\alpha)$ in the resolvent can be replaced by E_0, where $O(\alpha)$ represents possible energy shifts from lower-order terms that do *not* break the degeneracy and E_0 is the zeroth-order energy of the degenerate manifold of states.

2. Order of off-diagonal terms

Every order in DPT can, in principle, have diagonal (in the S_i^z basis) as well as off-diagonal terms in which the de-

generacy is removed. Any off-diagonal term in the effective Hamiltonian must flip spins in such a way as to preserve the 3:1 constraint on each tetrahedron. This can only be accomplished by flipping spins around a nontrivial closed loop on the pyrochlore lattice (see, e.g., Ref. 2). The smallest such loop involves flipping spins around a hexagonal plaquette from $S^z=\pm s$ to $S^z=\mp s$. This requires $\mathcal{H}_1$ to act $2s$ times, so off-diagonal processes occur first at order $O(J_\perp^{6s})$. Therefore, below this order of DPT, one need consider only diagonal terms. In Sec. III B, we will demonstrate that the lowest order diagonal energy splitting term for any s can occur only at sixth order. For spin $s=\frac{1}{2}$, an off-diagonal term appears at third order in DPT, and no diagonal energy splitting occurs at this order, resulting in a purely off-diagonal effective Hamiltonian. For spin $s=1$, the lowest-order diagonal and off-diagonal terms simultaneously appear at sixth order. For any higher value of s, the diagonal energy splitting appears at a lower order than any off-diagonal term can occur, and therefore the leading-order effective Hamiltonian is purely diagonal in the 3:1 states. We will nevertheless compute the first nonvanishing off-diagonal term for various values of s in Sec. V B to use its magnitude for an assessment of the validity of the truncation of the DPT expansion.

3. Unitarily transformed formalism for diagonal terms

We next develop a scheme to compute the diagonal terms by unitarily transforming the expression in Eq. (14) to obtain a formula for the diagonal effective Hamiltonian with all dependence upon the spin state explicit. The 3:1 manifold can be described using the Ising variables to indicate which spins are minority sites. That is, in the 3:1 states, we denote $S_j^z=\sigma_j s$, with $\sigma_j=\pm 1$ the Ising variable. At nth order, presuming that all lower-order terms are constants, the diagonal terms in the effective Hamiltonian constitute the function of the set $\{\sigma_i\}$ given by

$$\mathcal{H}_n[\{\sigma_i\}]=(-1)^{n+1}\langle\psi[\{\sigma_i\}]|(\mathcal{H}_1\mathcal{R}\mathcal{Q})^{n-1}H_1|\psi[\{\sigma_i\}]\rangle, \tag{15}$$

where the resolvent $\mathcal{R}=(\mathcal{H}_0-E_0)^{-1}$, $\mathcal{Q}=1-\mathcal{P}$, and

$$|\psi[\{\sigma_i\}]\rangle=\otimes_i|S_i^z=\sigma_i s\rangle. \tag{16}$$

The assumption that all lower-order terms are constant allows us to replace E by E_0 in the denominators in Eq. (14), since the constant corrections to E lead to higher-order terms in the effective Hamiltonian.

The dependence upon the σ_i in Eq. (15) is not explicit, but, following Hizi and Henley,[26] it can be made so by a unitary transformation. The operator

$$\hat{U}=\exp\left(+i\pi\sum_j\frac{(1-\sigma_j)}{2}\hat{S}_j^x\right) \tag{17}$$

effects a rotation about the x axis in spin space only for the minority spins. This interchanges raising and lowering operators and reverses the orientation of S_i^z for these sites. We may therefore write

$$|\psi[\{\sigma_i\}]\rangle=U|\psi_0\rangle, \tag{18}$$

where

$$|\psi_0\rangle=\otimes_i|S_i^z=s\rangle \tag{19}$$

is the fully polarized state, which is now independent of σ_i. Then, we have

$$\mathcal{H}_n[\{\sigma_i\}]=(-1)^{n+1}\langle\psi_0|(\tilde{\mathcal{H}}_1\tilde{\mathcal{R}}\tilde{\mathcal{Q}})^{n-1}\tilde{H}_1|\psi_0\rangle, \tag{20}$$

where

$$\tilde{\mathcal{O}}=U^\dagger\mathcal{O}U \tag{21}$$

for any operator $\mathcal{O}$. In what follows, all the operators appearing in Eq. (20) above will be simplified so that their dependence upon σ_i becomes explicit.

First consider $\tilde{\mathcal{H}}_1$. It consists, from Eq. (6), of a sum of operators transferring spin 1 between two nearest-neighbor sites, i.e., a bond of the pyrochlore lattice. We define the nearest-neighbor connectivity matrix of the lattice $\Gamma_{ij}=\Gamma_{ji}=1$ when i and j are nearest neighbors, and $\Gamma_{ij}=0$ otherwise. With this terminology, we write Eq. (6) as

$$\mathcal{H}_1=J_z\frac{\alpha}{4}\sum_{ij}\Gamma_{ij}(S_i^+S_j^-+\text{H.c.}). \tag{22}$$

After the unitary transformation, one obtains

$$\begin{aligned}\tilde{\mathcal{H}}_1=U^\dagger\mathcal{H}_1U&=J_z\frac{\alpha}{4}\sum_{ij}\Gamma_{ij}(S_i^{+\sigma_i}S_j^{-\sigma_j}+\text{H.c.})\\&=J_z\frac{\alpha}{4}\sum_{ij}\Gamma_{ij}\left[\frac{(1+\sigma_i\sigma_j)}{2}(S_i^+S_j^-+\text{H.c.})\right.\\&\quad\left.+\frac{(1-\sigma_i\sigma_j)}{2}(S_i^+S_j^++\text{H.c.})\right].\end{aligned} \tag{23}$$

Here, the expressions $(1\pm\sigma_i\sigma_j)/2$ denote "Ising delta functions" that select the cases in which the two $\sigma_{i,j}$ have the same or opposite signs.

Assuming that the lowest-order term in DPT that splits the 3:1 configurations is a diagonal term of order n_0, the only 3:1 configuration which can be reached as an intermediate state in Eq. (15) for any $n\leqslant n_0$ is the starting state $|\psi[\{\sigma_i\}]\rangle$. Under the unitary transformation, this state maps to $|\psi_0\rangle$, and therefore the projection operator $\tilde{\mathcal{Q}}$ may be replaced by

$$\tilde{\mathcal{Q}}\to 1-|\psi_0\rangle\langle\psi_0| \tag{24}$$

in Eq. (20).

Finally, we consider the resolvent. Using $U^\dagger S_i^zU=\sigma_iS_i^z$, one finds

$$\tilde{\mathcal{R}}^{-1}=\frac{J_z}{2}\sum_{ij}\Gamma_{ij}\sigma_i\sigma_jS_i^zS_j^z-2J_zh\sum_j\sigma_jS_j^z-E_0. \tag{25}$$

First, we note that because both $\mathcal{H}_0$ and $\mathcal{H}_1$ conserve the total magnetization of the lattice [this is just the conserved quantity arising from the global U(1) symmetry], the term $\Sigma_j\sigma_jS_j^z$ remains unchanged at every stage in a DPT process, and we can therefore absorb this term into the constant energy E_0. Clearly, the inverse resolvent should vanish when acting upon the fully polarized state $|\psi_0\rangle$. Hence, we may absorb the constant energy E_0 into the sum as

$$\tilde{\mathcal{R}}^{-1} = \frac{J_z}{2}\sum_{ij} \Gamma_{ij}\sigma_i\sigma_j(S_i^z S_j^z - s^2). \tag{26}$$

We can simplify the resolvent in the restricted space of virtual states, which will be accessed in evaluating Eq. (20). In particular, the σ_i configurations are restricted to the 3:1 manifold. Furthermore, we note that all intermediate states will have only some small finite set of spins whose S_i^z quantum numbers are different from s due to the action of $\tilde{H}_1$. Let us consider then the action of the resolvent on a state for which this set of sites is denoted by F. In this case, only terms in Eq. (26) for which at least one of i or j is in F can contribute. Thus,

$$\tilde{\mathcal{R}}^{-1} = \frac{J_z}{2}\sum_{ij\in\mathsf{F}} \Gamma_{ij}\sigma_i\sigma_j(S_i^z S_j^z - s^2) + J_z s\sum_{i\in\mathsf{F}}\sum_{j\notin\mathsf{F}} \Gamma_{ij}\sigma_i\sigma_j(S_i^z - s). \tag{27}$$

One may replace the sum over j by $\Sigma_{j\notin\mathsf{F}} = \Sigma_j - \Sigma_{j\in\mathsf{F}}$ to obtain

$$\tilde{\mathcal{R}}^{-1} = \frac{J_z}{2}\sum_{ij\in\mathsf{F}} \Gamma_{ij}\sigma_i\sigma_j(S_i^z - s)(S_j^z - s) + J_z s\sum_{i\in\mathsf{F}} \sigma_i\left(\sum_j \Gamma_{ij}\sigma_j\right)(S_i^z - s). \tag{28}$$

The crucial observation is that the 3:1 constraint implies

$$\sum_j \Gamma_{ij}\sigma_j = 4 - 2\sigma_i. \tag{29}$$

This is because once σ_i is specified, the set of its neighbors is also specified (see also Fig. 3). Equation (29) allows one to eliminate the latter sum and obtain

$$\tilde{\mathcal{R}}^{-1} = \frac{J_z}{2}\sum_{ij\in\mathsf{F}} \Gamma_{ij}\sigma_i\sigma_j(S_i^z - s)(S_j^z - s) + 2J_z s\sum_{i\in\mathsf{F}} (2\sigma_i - 1)(S_i^z - s). \tag{30}$$

Using again the observation that $\Sigma_j \sigma_j S_j^z$ remains unchanged throughout the stages of any DPT process, it is equal to the constant $\Sigma_j \sigma_j S_j^z = \Sigma_j \sigma_j s$. Using this fact, we finally obtain

$$\tilde{\mathcal{R}}^{-1} = \frac{J_z}{2}\sum_{ij\in\mathsf{F}} \Gamma_{ij}\sigma_i\sigma_j(S_i^z - s)(S_j^z - s) - 2J_z s\sum_{i\in\mathsf{F}} (S_i^z - s). \tag{31}$$

By successive action of $\tilde{\mathcal{H}}_1$, $\tilde{\mathcal{Q}}$, and $\tilde{\mathcal{R}}$ using Eqs. (23), (24), and (31), one can obtain explicit expressions for any intermediate state in the DPT expression of Eq. (20) with $n \leqslant n_0$. For example, one action of each of these operators gives

$$\tilde{\mathcal{R}}\tilde{\mathcal{Q}}\tilde{\mathcal{H}}_1|\psi_0\rangle = \frac{\alpha s}{4(4s-1)}\sum_{a_1 a_2} \Gamma_{a_1 a_2}(1 - \sigma_{a_1}\sigma_{a_2})|1_{a_1}1_{a_2}\rangle, \tag{32}$$

where we have introduced the compact notation

$$|(m_1)_{a_1}\cdots(m_n)_{a_n}\rangle = |S_{a_1}^z = s - m_1\rangle\cdots|S_{a_n}^z = s - m_n\rangle \otimes_{i\neq a_1\cdots a_n}|S_i^z = s\rangle. \tag{33}$$

Acting twice with the same sequence of operators gives

$$\begin{aligned}(\tilde{\mathcal{R}}\tilde{\mathcal{Q}}\tilde{\mathcal{H}}_1)^2|\psi_0\rangle = {} & \frac{\alpha^2 s}{16(4s-1)}\sum_{a_1 a_2} \Gamma_{a_1 a_2}(1 - \sigma_{a_1}\sigma_{a_2})|2_{a_1}2_{a_2}\rangle + \frac{\alpha^2 s^2}{4(4s-1)}\sum_{a_1 a_2 a_3} \frac{\Gamma_{a_1 a_3}\Gamma_{a_2 a_3}\eta_{a_1 a_2}}{4s - \Gamma_{a_1 a_2}}[(\sigma_{a_1} + \sigma_{a_3})\sigma_{a_2} - \sigma_{a_1}\sigma_{a_3} - 1]|1_{a_1}1_{a_2}\rangle \\ & + \frac{\alpha^2 s^{3/2}\sqrt{2s-1}}{4(4s-1)}\sum_{a_1 a_2 a_3} \frac{\Gamma_{a_1 a_2}\Gamma_{a_1 a_3}\eta_{a_2 a_3}}{8s - 4 + \Gamma_{a_2 a_3}}[1 + \sigma_{a_2}\sigma_{a_3} - \sigma_{a_1}(\sigma_{a_2} + \sigma_{a_3})]|2_{a_1}1_{a_2}1_{a_3}\rangle \\ & + \frac{\alpha^2 s^2}{16(4s-1)}\sum_{a_1\cdots a_4} \frac{\Gamma_{a_1 a_2}\Gamma_{a_3 a_4}\eta_{a_1 a_4}\eta_{a_2 a_3}\eta_{a_2 a_4}}{8s - 2 + \sigma_{a_1}\sigma_{a_3}(\Gamma_{a_1 a_3} - \Gamma_{a_1 a_4} - \Gamma_{a_2 a_3} + \Gamma_{a_2 a_4})}(1 - \sigma_{a_1}\sigma_{a_2})(1 - \sigma_{a_3}\sigma_{a_4})|1_{a_1}1_{a_2}1_{a_3}1_{a_4}\rangle,\end{aligned} \tag{34}$$

where we have introduced the "noncoincident" symbol

$$\eta_{ab} = 1 - \delta_{ab}. \tag{35}$$

The corresponding expressions for more successive actions of these operators upon $|\psi_0\rangle$ can also be obtained but are too unwieldy to present here.

Using such expressions, one may readily evaluate the terms $\mathcal{H}_n[\{\sigma_i\}]$ in the diagonal effective Hamiltonian, Eq. (20). For n_0 an even number, a convenient way to calculate the n_0th order term is to consider the state

$$|\Psi\rangle = \tilde{\mathcal{R}}^{1/2}\tilde{\mathcal{Q}}\tilde{\mathcal{H}}_1(\tilde{\mathcal{R}}\tilde{\mathcal{Q}}\tilde{\mathcal{H}}_1)^{n_0/2-1}|\psi_0\rangle \tag{36}$$

and then find the magnitude of this wave function:

$$\mathcal{H}_{n_0}[\{\sigma_i\}] = -\langle\Psi|\Psi\rangle. \tag{37}$$

Note that the square root of $\tilde{\mathcal{R}}$ in Eq. (36) is easily evaluated by just taking the square root of Eq. (31), since it is diagonal

in the basis of 3:1 configurations. Other terms can be obtained similarly.

B. Restricting the Hilbert space to the 3:1 manifold

Calculating each such magnitude as defined in the previous section leads to an explicit expression for the corresponding term in DPT. These expressions appear to be extremely complex and formidable functions of the Ising spin variables $\{\sigma_i\}$. In this section, we show that the projection of these functions to the 3:1 manifold of allowed $\{\sigma_i\}$ configurations affords a tremendous simplification. In fact, we will demonstrate that all terms in DPT below sixth order can give only constant functions—i.e., no splitting—within the 3:1 states. At sixth order, the full functional dependence can be characterized by only three independent numbers which may be defined on plaquettes of the pyrochlore lattice. We show how these numbers can be extracted from the expressions obtained by the analysis of the previous subsection.

1. Functional form of diagonal DPT terms

From the analysis of the previous section, the nth-order effective diagonal Hamiltonian in DPT must take the form of a multiple sum of n site indices $a_1 \ldots a_n$, where each site index is summed over all lattice sites. The summand is a function only of s and of the set of σ_i, Γ_{ij}, η_{ij}, and δ_{ij}, where i and j must *belong* to the set of the site indices. The general form can be somewhat simplified by noting first that the dependence upon the η_{ij} can be eliminated by rewriting them in terms of δ_{ij} using Eq. (35), and then eliminating all δ_{ij} by collapsing the sums containing these factors. Finally, we note that any factors of Γ_{ij} in the denominators in these expressions can be moved to the numerator using the identity

$$g(\Gamma_{ij}) = g(0) + \Gamma_{ij}[g(1) - g(0)], \tag{38}$$

for any function g (which may also depend upon any other set of variables), since $\Gamma_{ij}=0,1$.

By these manipulations, one may write the effective Hamiltonian $\mathcal{H}_{\text{eff}}[\{\sigma_i\}]=\Sigma_n \mathcal{H}_n[\{\sigma_i\}]$ as

$$\mathcal{H}_{\text{eff}}[\{\sigma_i\}] = \sum_n \sum_{G_n} \sum_{a_1,\ldots,a_n} \left(\prod_{(ij)\in G_n} \Gamma_{a_i a_j} \right) f_{G_n}(\sigma_{a_1}, \ldots, \sigma_{a_n}). \tag{39}$$

Here, we have divided the effective Hamiltonian into terms involving n independent site variables $a_1, \ldots, a_n$ that are summed over the lattice sites. A given order N in DPT contributes terms with $n \leqslant N$. For a given n, all possible products of $\Gamma_{a_i a_j}$ can appear. The different such products are specified by G_n, which may be considered as a "diagram" in the following fashion. Each G_n can be represented by drawing n points, corresponding to $i=1, \ldots, n$, and connecting some arbitrary set of pairs of these points by lines. For each (unordered) pair of points (ij), which is connected in G_n, we include one factor of $\Gamma_{a_i a_j}$. Since there are $n(n-1)/2$ pairs of points, and each pair may or may not be connected, there are $2^{n(n-1)/2}$ distinct diagrams G_n. For example, in our conventions, $\Gamma_{a_1 a_2}\Gamma_{a_2 a_3}\Gamma_{a_3 a_4}$ and $\Gamma_{a_1 a_2}\Gamma_{a_2 a_3}\Gamma_{a_3 a_5}$ are represented by different diagrams (see Fig. 1), which means that

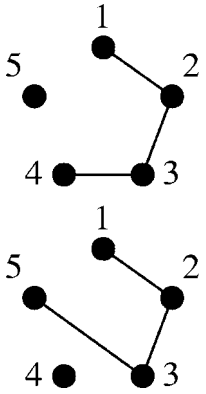

FIG. 1. Examples of contractible diagrams.

$f_{G_n}(\sigma_{a_1}, \ldots, \sigma_{a_6})$ is not necessarily symmetric with respect to swapping σ_{a_4} and σ_{a_5}. We will refer to the number n as the *order* of the given term, even though it can come from a term of that order or higher in DPT.

2. Contractible diagrams

First, we would like to show that any such term represented by a diagram containing a point i with less than two connections to other points can be reduced to a term of one lower order. These diagrams are "contractible" (see Fig. 2 for examples). We prove this by showing that the sum over a_i can be carried out explicitly to obtain an expression of the same form of Eq. (39) in terms of the $n-1$ remaining sum variables. There are two cases. Suppose in G_n the point i in question has no lines connected to it. Taking $i=n$ without loss of generality, we note that the sum on a_n is unconstrained, i.e., it runs over all lattice sites. Thus we may write

$$\begin{aligned} 2\sum_{a_n} f_{G_n}(\sigma_{a_1}, \ldots, \sigma_{a_n}) &= \sum_t \sum_{a\in t} f_{G_n}(\sigma_{a_1}, \ldots, \sigma_a) \\ &= N_t[3 f_{G_n}(\sigma_{a_1}, \ldots, \sigma_{a_{n-1}}, +) \\ &\quad + f_{G_n}(\sigma_{a_1}, \ldots, \sigma_{a_{n-1}}, -)]. \end{aligned} \tag{40}$$

The second line applies because on every tetrahedron there is the same set of four single-spin states. By inserting Eq. (40) into Eq. (39), one reduces the order of this term, as asserted above.

Consider the second case in which there is one connection to the point $i=n$. We may suppose that this connection is to the point $j<n$. The sum over a_n is then constrained *only* by the requirement that a_n be a nearest neighbor of a_j. For fixed a_j, this includes just six sites on the pyrochlore lattice. More-

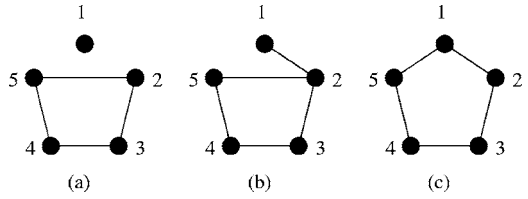

FIG. 2. Examples of contractible [(a) and (b)] and noncontractible (c) diagrams.

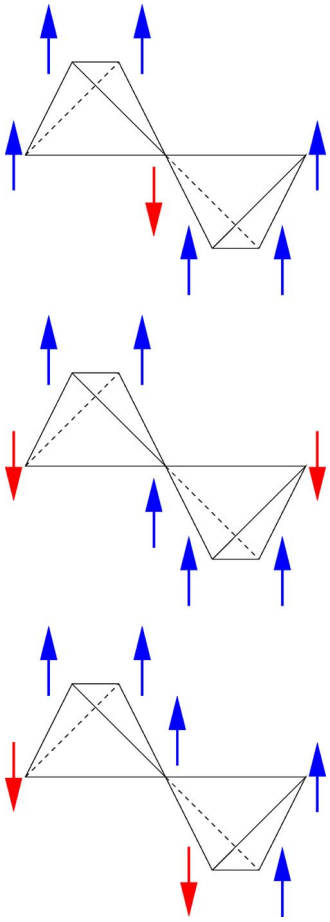

FIG. 3. (Color online) The three possible configurations of minority sites (down-pointing red arrow) on two adjacent tetrahedra in the 3:1 manifold of states.

over, the set of spins on these six sites is entirely determined by the spin at site a_j. In particular, if $\sigma_{a_j}=+1$, the sum contains four terms with $\sigma_{a_n}=+1$ and two terms with $\sigma_{a_n}=-1$; if $\sigma_{a_j}=-1$, the sum contains six spins with $\sigma_{a_n}=+1$. This can easily be understood from Fig. 3. Therefore, the sum can again be carried out explicitly as follows:

$$\sum_{a_n} \Gamma_{a_n a_j} f_{G_n}(\sigma_{a_1}, \ldots, \sigma_{a_n}) = \frac{1+\sigma_{a_j}}{2}[4 f_{G_n}(\sigma_{a_1}, \ldots, +) + 2 f_{G_n}(\sigma_{a_1}, \ldots, -)] + \frac{1-\sigma_{a_j}}{2} 6 f_{G_n}(\sigma_{a_1}, \ldots, \sigma_{a_{n-1}}, +). \tag{41}$$

Once again, Eq. (41) can be inserted into Eq. (39) to reduce the order by 1.

3. Noncontractible diagrams

Since all contractible diagrams can be reduced using the above rules until they become either noncontractible or constant, we therefore need to consider only noncontractible diagrams. In these diagrams, each point in G_n is connected to at least two other points. Let us first make a few general observations about these diagrams. One can readily see that for these diagrams at order $n \leqslant 5$, all points must be connected, i.e., it is possible to pass from one point to an other by a sequence of links. It is useful to consider the notion of a *loop*, or sequence of points, each connected to the next by a link, which visits no point twice and returns to the first point of the sequence. For $n \leqslant 4$, there is always at least one loop which includes all n points. For $n=5$, all but three noncontractible diagrams contain a loop of length 5. The three remaining diagrams at $n=5$ contain smaller loops [see part (c) of Fig. 4]. All the noncontractible single loop diagrams for $n \leqslant 5$ are shown in Fig. 4. For $n=6$, there is one possible *disconnected* diagram, which contains two disjoint loops of length 3. Apart from this last diagram, all others are fully connected.

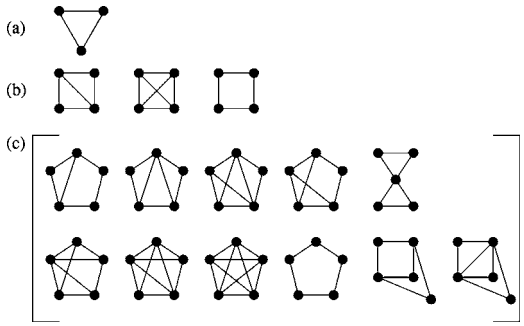

FIG. 4. All $n \leqslant 5$ noncontractible diagrams. (a) The triangle diagram is the only possible such diagram for $n=3$. (b) The square-framed diagrams are all the possibilities for $n=4$. (c) The pentagon-framed diagrams together with the three rightmost diagrams comprise all the possibilities for $n=5$.

Let us consider the physical pyrochlore sites which are summed over in a given term. They comprise a set $\mathsf{S}(G_n)=\{(a_1^{(1)}, \ldots, a_n^{(1)}), (a_1^{(2)}, \ldots, a_n^{(2)}), \ldots\}$ of solutions $(a_1^{(i)}, \ldots, a_n^{(i)})$, to the conditions

$$\Gamma_{a_i a_j} = 1 \quad \text{for } (ij) \in G_n. \tag{42}$$

We will call these solutions "clusters." In an infinite system, S is, of course, infinite because of translational symmetry, but this is immaterial. A given term may then be written simply as

$$\sum_{(a_1, \ldots, a_n) \in \mathsf{S}(G_n)} f(\sigma_{a_1}, \ldots, \sigma_{a_n}). \tag{43}$$

We note that all the clusters for $n \leqslant 5$ are confined to one or two adjacent tetrahedra. This can be seen by considering the constraints imposed on clusters by the noncontractibility of the diagram. For instance, all but three diagrams at order $n=5$ contain a loop of length 5, and this allows only three topologies of clusters, which are illustrated in Fig. 5. The remaining three diagrams only allow clusters that are confined to two or less adjacent tetrahedra. We will show more generally that any term containing only clusters confined to three or fewer adjacent tetrahedra is a constant.

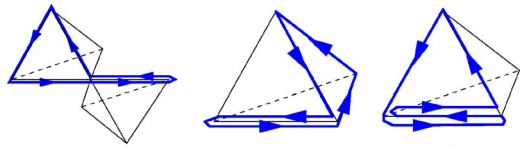

FIG. 5. (Color online) Three example topologies of closed paths of five steps on the pyrochlore lattice. These are all the possible topologies of clusters corresponding to diagrams at order $n=5$ containing a loop of length 5.

The set S can therefore be broken up into three components, comprising clusters which contain 1, 2, or only 3 multiply occupied tetrahedra,

$$\mathsf{S}(G_n) = \mathsf{S}_1(G_n) + \mathsf{S}_2(G_n) + \mathsf{S}_3(G_n). \tag{44}$$

The sum in Eq. (43) can be carried out separately over these three sets. Let us consider first the sum over S_1. The clusters in S_1 can be divided into subsets of those residing on a specific tetrahedron S_1^t.

An arbitrary permutation P of the four sites on tetrahedron t leaves the set $\mathsf{S}_1^t(G_n)$ invariant. This is because each solution obeys Eq. (42), and $\Gamma_{a_i a_j}=\Gamma_{P(a_i)P(a_j)}$ for $a_i, a_j \in t$ (this is a set of permutations that leaves nearest-neighbor pairs invariant).

The contribution of all clusters on t to the term in question can only be a function of the four Ising variables of the four sites $q=1,2,3,4 \in t$,

$$\sum_{(a_1,\ldots,a_n)\in \mathsf{S}_1^t} f_{G_n}(\sigma_{a_1},\ldots,\sigma_{a_n}) = F(\sigma_1,\sigma_2,\sigma_3,\sigma_4). \tag{45}$$

Now, we can use the fact that the spin configurations on one tetrahedron are always constrained to be of the 3:1 form, i.e., they are a permutation P of the specific configuration $+\ +\ +\ -$:

$$\sigma_q = \sigma^0_{P(q)}, \tag{46}$$

with $(\sigma^0_1,\sigma^0_2,\sigma^0_3,\sigma^0_4)=(+,+,+,-)$. Here $q\to P(q)$ is a permutation of the four sites. The specific (cyclic) permutation P now encodes the spin state on this tetrahedron,

$$\begin{aligned} F(\sigma^0_{P(1)},\sigma^0_{P(2)},\sigma^0_{P(3)},\sigma^0_{P(4)}) &= \sum_{(a_1,\ldots,a_n)\in \mathsf{S}_1^t} f_{G_n}(\sigma^0_{P(a_1)},\ldots,\sigma^0_{P(a_n)}) \\ &= \sum_{(a_1,\ldots,a_n)\in P^{-1}(\mathsf{S}_1^t)} f_{G_n}(\sigma^0_{a_1},\ldots,\sigma^0_{a_n}). \end{aligned} \tag{47}$$

Since the set $\mathsf{S}_1^t(G_n)$ is invariant under these permutations, we find from the last expression that $F(\sigma_1,\sigma_2,\sigma_3,\sigma_4)$ is also invariant under the permutations. Hence, this contribution is identical for *all* spin configurations and is a constant within the 3:1 manifold.

Let us next consider the clusters in S_2. For each cluster, there are two neighboring tetrahedra t and t', each of which contains two or more sites a_i. These tetrahedra share one specific site, which we call A. The pair of tetrahedra in question are determined by A (the tetrahedra t and t' are determined by the choice of A). For one such cluster, the sites a_i with $i=1,\ldots,n$ may be partitioned into three groups: the site A and those which are on t or t' but are not A:

$$\bar{t} = t - \{A\}, \tag{48}$$

$$\bar{t}' = t' - \{A\}. \tag{49}$$

Similarly to S_1, we can divide S_2 into subsets S_2^A residing on tetrahedron pairs defined by the site A. We can then rewrite the sum by summing A over all lattice sites and summing the set of sites $a_1,\ldots,a_n$ over S_2^A,

$$\begin{aligned} &\sum_{(a_1,\ldots,a_n)\in \mathsf{S}_2} f_{G_n}(\sigma_{a_1},\ldots,\sigma_{a_n}) \\ &\quad = \sum_A \sum_{(a_1,\ldots,a_n)\in \mathsf{S}_2^A} f_{G_n}(\sigma_{a_1},\ldots,\sigma_{a_n}). \end{aligned} \tag{50}$$

We now observe that the set of solutions S_2^A is invariant under any permutation P_t ($P_{t'}$) of the three sites in $\bar{t}$ ($\bar{t}$). This is exactly as for S_1^t because each solution in S_2^A obeys Eq. (42), and $\Gamma_{a_i a_j}=\Gamma_{P_t(a_i)P_t(a_j)}$ for $a_i, a_j \in A\cup\bar{t}\cup\bar{t}'$ (and the same holds if P_t is replaced by $P_{t'}$).

The sum

$$\sum_{(a_1,\ldots,a_n)\in \mathsf{S}_2^A} f_{G_n}(\sigma_{a_1},\ldots,\sigma_{a_n}) \tag{51}$$

can only be a function of the seven Ising variables of the sites in $A\cup\bar{t}\cup\bar{t}'$. Due to the 3:1 constraint, if $\sigma_A=+$, then the Ising variables σ_q for $q\in\bar{t}$ must be a permutation P_t of $\sigma^{(1)}_q=(++-)$. If $\sigma_A=-$, then all the $\sigma_q=+$. Hence, we may write

$$\sigma_q = \begin{cases} \dfrac{(1+\sigma_A)}{2}\sigma^{(1)}_{P_t(q)} + \dfrac{(1-\sigma_A)}{2}(+1) & \text{for } q\in\bar{t} \\ \dfrac{(1+\sigma_A)}{2}\sigma^{(1)}_{P_{t'}(q)} + \dfrac{(1-\sigma_A)}{2}(+1) & \text{for } q\in\bar{t}'. \end{cases} \tag{52}$$

Using these expressions and the fact that S_2^A is invariant under these two permutations, the sum in Eq. (51) is found to depend only on σ_A.

This finally leaves

$$\sum_{(a_1,\ldots,a_n)\in \mathsf{S}_2} = \sum_A \tilde{f}(\sigma_A), \tag{53}$$

where $\tilde{f}(\sigma_A)$ is a complicated function obtained from the above manipulations—which, however, does not depend upon A itself. The sum is clearly then constant, as the number of $+$ and $-$ spins are fixed for the lattice. Thus, all terms in S_2 are also constants.

Finally, consider S_3. In these clusters, there are three adjoining tetrahedra, and one may identify a "central" tetrahedron t which shares a site with each of the other two tetrahedra t' and t''. Here, one may divide the sum variables into five groups: two corresponding to the site shared by t and t' and the site shared by t and t'' and three others corresponding to the sites on t, t', and t'' but not shared. One can again sum

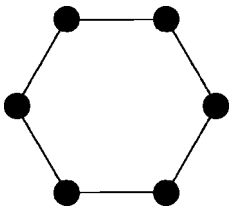

FIG. 6. The only diagram at order $n=6$ giving a nonconstant diagonal contribution in degenerate perturbation theory.

over the unshared sites on t' and t'' and obtain an expression for the cluster sum, which involves sites only on t. By manipulations of the type used to analyze S_1, one finds that this remaining single-tetrahedron sum must also be constant.

We conclude that any term for which the corresponding clusters are confined to three or fewer adjacent tetrahedra must be constant. Therefore, all terms up to and including fifth order are constant. At sixth order, among the noncontractible diagrams, there are a few exceptions. First, there is one disconnected diagram containing two loops of length 3. In this term, the sum over variables in the first and second groups is independent, and, therefore, each can be carried out separately as for a third-order term. This immediately gives a constant contribution. The remaining diagrams are connected. All but one of these diagrams contains a loop of length 5 or less (possibly in addition to other larger loops). Such terms are confined to three or fewer tetrahedra and are constant by the above arguments. What remains is the single diagram consisting of only a single loop of length 6, as shown in Fig. 6.

This "large loop" diagram is thus the sole nontrivial contribution. It can be written in the form

$$\mathcal{H}_6^L[\{\sigma_i\}] = \sum_{a_1 \ldots a_6} \left(\prod_{i=1}^{6} \Gamma_{a_i a_{i+1}} \right) f_L(\sigma_{a_1}, \ldots, \sigma_{a_6}), \quad (54)$$

where we identify $a_7=a_1$. To analyze each term (given a particular set $a_1, \ldots, a_6$), we employ a trick: multiplying it by a carefully chosen representation of the identity

$$1 = \prod_{\langle\langle ij \rangle\rangle} (\delta_{a_i a_j} + \eta_{a_i a_j}), \quad (55)$$

with $\eta_{ab}=1-\delta_{ab}$. Here, the product is over distinct pairs i,j, which are not connected in the loop diagram. We multiply the loop term by this expression and expand the product fully. All but one term involves at least one Kronecker δ function. In each of these summand terms, at least one sum can be collapsed, leading to a lower-order term, which is necessarily a constant as we have already shown. The remaining nonvanishing part is the original summand term multiplied by the product,

$$\prod_{\langle\langle ij \rangle\rangle} \eta_{a_i a_j}. \quad (56)$$

This factor is nonzero if and only if all $n=6$ sites a_i are *distinct*. Thus, the sites a_i must comprise a closed walk on the lattice in which each site on the walk is visited only once. On the pyrochlore lattice, this is exactly the set of hexagonal plaquettes. A specific plaquette on the lattice containing sites $i_1, \ldots, i_6$ in sequence around the plaquette appears 12 times in the sum in Eq. (54), with $a_1, \ldots, a_6$ taking the six cyclic permutations of $i_1, \ldots, i_6$ and the six cyclic permutations of these sites in reverse order. Hence, the nonconstant contribution to the diagonal energy at sixth order in DPT can be written as

$$\mathcal{H}_6 = \sum_{\mathcal{P}} \mathcal{E}_P(i_1, \ldots, i_6), \quad (57)$$

where $i_1, \ldots, i_6$ are the six sites moving clockwise around plaquette $\mathcal{P}$ and

$$\mathcal{E}_P(\sigma_{i_1}, \ldots, \sigma_{i_6}) = \sum_{k=1}^{6} [f_L(\sigma_{i_k}, \ldots, \sigma_{i_{k+5}}) + f_L(\sigma_{i_{k+5}}, \ldots, \sigma_{i_k})], \quad (58)$$

where $i_{k+6} \equiv i_k$.

TABLE I. The different plaquette types, with the fraction of minority sites in each one.

Type	Configuration	Fraction of minority spins
0	↑↑↑↑↑↑	0
1	↓↑↓↑↓↑	$\frac{1}{2}$
2	↓↑↑↑↑↑	$\frac{1}{6}$
3	↓↑↓↑↑↑	$\frac{1}{3}$
4	↓↑↑↓↑↑	$\frac{1}{3}$

C. Results

We have carried out the calculations detailed in the previous sections. Specifically, by explicitly constructing $|\Psi\rangle$ in Eq. (36), we obtained $\mathcal{H}_6[\{\sigma_i\}]$ in Eq. (37). From this, we extracted the function f_L in Eq. (54) and thereby determined the plaquette energies $\mathcal{E}_\mathcal{P}$ using Eq. (58). Using the 3:1 constraint, there are five configurations possible on any plaquette, which we denote "type 0" to "type 4." These are enumerated in Table I. The DPT calculation gives a specific energy (proportional to $J_z\alpha^6$) for each type.

There is some freedom in the choice of these five energies. That is, certain changes of the plaquette energies leave the *differences* of total energy among distinct 3:1 states unchanged. One such obvious "gauge" change is a global shift of all five energies by the same amount. Another less obvious constraint comes directly from the 3:1 rule. If one denotes the fraction of plaquettes in the lattice in configuration a by x_a, the total fraction of minority sites must always be 1/4. Each plaquette configuration has a fixed fraction of minority sites M_a, given in Table I. Thus,

$$\frac{1}{4} = \sum_{a=0}^{4} M_a x_a. \quad (59)$$

The energy per plaquette is then

$$\mathcal{H}_6 = \sum_{a=0}^{4} \mathcal{E}_a x_a. \tag{60}$$

Using Eq. (59), one sees that a shift $\Delta E_a = cM_a$, with arbitrary constant c, shifts the energy by a constant. The obvious global energy shift remarked above derives similarly from the normalization condition $\Sigma_a x_a = 1$. Using these two constraints, we see that there are only three independent plaquette fractions. We (arbitrarily) choose to keep $x_{1,2,4}$ as our independent variables. Substituting the solutions for the other fractions ($x_{0,3}$) into Eq. (60), we find

$$\mathcal{H}_6 = x_1 V_1 + x_2 V_2 + x_4 V_4, \tag{61}$$

with the three "gauge invariant" physical energy parameters

$$V_1 = \frac{1}{2}(\mathcal{E}_0 + 2\mathcal{E}_1 - 3\mathcal{E}_3),$$

$$V_2 = \frac{1}{2}(-\mathcal{E}_0 + 2E_2 - \mathcal{E}_3),$$

$$V_4 = (\mathcal{E}_4 - \mathcal{E}_3). \tag{62}$$

Our DPT results are

$$V_1 = -J_z \alpha^6 \frac{3s^4(98\,304s^5 - 139\,648s^4 + 79\,136s^3 - 22\,040s^2 + 3006s - 165)}{32(2s-1)(4s-1)^5(8s-3)^2(12s-5)},$$

$$V_2 = J_z \alpha^6 \frac{s^3(256s^3 - 51s + 9)}{32(4s-1)^3(8s-3)^2},$$

$$V_4 = J_z \alpha^6 \frac{s^4(272s^2 - 136s + 15)}{16(4s-1)^5(8s-3)^2}. \tag{63}$$

We have made several checks on the above calculation. First, we have carried out a more direct scheme, which sums the terms in DPT in a completely different manner from the methods described in this section. We leave the vast details of this calculation to Appendix B. The results of this alternative method agree perfectly with those quoted above. Second, in the following section, we will compare the $s \to \infty$ limit of the above result with the result of a large-s calculation for the XXZ model. The large-s limit of the energies we find in DPT becomes

$$\lim_{s\to\infty} \frac{V_1}{s} = 0,$$

$$\lim_{s\to\infty} \frac{V_2}{s} = \frac{J_z \alpha^6}{512},$$

$$\lim_{s\to\infty} \frac{V_4}{s} = 0. \tag{64}$$

We shall see that this result indeed agrees exactly with the corresponding limit of the large-s expansion.

D. Off-diagonal term

In this section, we describe how the lowest-order off-diagonal term in the DPT effective Hamiltonian is calculated. As explained in Sec. III A 1, this term appears at order $O(\alpha^{6s})$.

The lowest-order off-diagonal term acts only on a hexagonal plaquette in the flippable configuration (type 1 plaquette, as in Table I). It changes the plaquette configuration from one flippable configuration to the other flippable configuration. Therefore, the off-diagonal term has the following general form:

$$\mathcal{H}_{\text{off diagonal}} = (-1)^{6s+1} \alpha^{6s} J_z K \sum_P \left(|\hexagon\rangle\langle\hexagon| + \text{H.c.} \right)$$

$$= (-1)^{6s+1} \alpha^{6s} J_z K \sum_P \left(|\downarrow\uparrow\downarrow\uparrow\downarrow\uparrow\rangle\langle\uparrow\downarrow\uparrow\downarrow\uparrow\downarrow| + \text{H.c.} \right), \tag{65}$$

where we denote the two flippable configurations of the plaquette by $|\hexagon\rangle$ and $\langle\hexagon|$ for the sake of brevity. Note that we can change the $(-1)^{6s+1}$ factor into a (-1) by a unitary transformation similar to that employed in Ref. 2. We shall now describe how the coefficient K is calculated.

Each of the DPT processes contributing to the off-diagonal term at this order consists of $2s$ spin transfer operations along the links of a hexagonal plaquette. In every such process, three spins go from an initial state of $+s$ to $-s$, and three start with $-s$ and end up as $+s$. We can calculate K by adding the contributions from all the DPT processes occurring on a single plaquette, starting in the state $|\downarrow\uparrow\downarrow\uparrow\downarrow\uparrow\rangle$ and ending in the state $|\uparrow\downarrow\uparrow\downarrow\uparrow\downarrow\rangle$.

The spins change via ladder operators $S_j^{\pm}$, and, therefore, we get the Clebsch-Gordan coefficients from the action of these operators. The same set of operators $S_j^{\pm}$ act in every process, $(S_1^+)^{2s}(S_2^-)^{2s}(S_3^+)^{2s}(S_4^-)^{2s}(S_5^+)^{2s}(S_6^-)^{2s}$ (the indices $1,\ldots,6$ denote the six sites around the hexagonal plaquette, as in Fig. 7), and so these factors are always the same. For the S^+ operators taking a single site from $-s$ to $+s$, we find

$$\prod_{m=-s}^{s-1} \sqrt{s(s+1) - m(m+1)} = (2s)!, \tag{66}$$

and for the S^- operators taking a single site from $+s$ to $-s$, we find

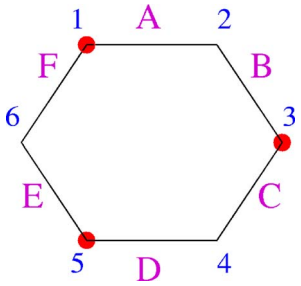

FIG. 7. (Color online) Notation for the off-diagonal processes on a single plaquette. The (red) circles denote minority sites. The sites are numbered (blue) 1,…,6, and the links are denoted by the (purple) $A,\ldots,F$.

$$\prod_{m=-s+1}^{s} \sqrt{s(s+1)-m(m-1)} = (2s)!. \tag{67}$$

In total from all the ladder operators, we find a common factor $((2s)!)^6$. From the six spin transfer operators, we have another common factor of $1/2^{6s}$.

All that remains to be calculated for a single DPT process is the product of resolvents of each stage in the spin transfer process. First let us classify the different processes on a single plaquette. Let us denote the six links of the plaquette by $A,\ldots,F$, as illustrated in Fig. 7. In order to get the right number of ladder operators S_1^+, the total number of times a spin transfer occurs on the two adjacent links sharing site 1 must add up to $N_A+N_F=2s$ (here N_X is the number of spin transfer operators acting on the link X in the DPT process). The same argument applies to all six sites around the plaquette. Next, consider the two equations

$$N_A + N_B = 2s,$$

$$N_B + N_C = 2s, \tag{68}$$

which imply that $N_A=N_C$. Repeating this argument for all the links around the plaquette, we find that we must have

$$N_A = N_C = N_E,$$

$$N_B = N_D = N_F, \tag{69}$$

in addition to the constraint $N_A+N_B=2s$, so that there is only one free parameter $N_A=0,\ldots,2s$, which we will use to classify the DPT processes.

Beyond determining the number N_A, the DPT processes further differ by the order in which the spin transfer operators act on the predetermined links. Each process is described by a string of $6s$ letters $q_1,\ldots,q_{6s}$, which contain N_A instances of each one of the three letters A, C, and E, and $2s-N_A$ instances of each one of B, D, and F. For example, a few possible strings for $s=1$ are $AACCEE$, $ABCDEF$, and all their permutations. From this classification, it is evident that in total there are $\Sigma_{N_A=0}^{2s}\{(6s)!/(N_A!)^3[(2s-N_A)!]^3\}$ different processes.

At this point, we can write a formal expression for the coefficient K as follows:

$$K = \frac{((2s)!)^6}{2^{6s}} \sum_{\{q_n\}} \prod_{\ell=1}^{6s-1} \tilde{\mathcal{R}}_\ell(\{q_n\}), \tag{70}$$

where $\tilde{\mathcal{R}}_\ell(\{q_n\})$ denotes the resolvent at step ℓ of the DPT process described by the string $\{q_n\}$.

Now, we turn to formulating the resolvent in a convenient manner that will facilitate the summation over all processes. Starting from Eq. (31), in this case, the set F consists only of the six sites surrounding the hexagonal plaquette $1,\ldots,6$. Since the six sites have alternating initial states $\pm s$, any pair of nearest-neighbor sites has $\sigma_i\sigma_j=-1$. We can therefore rewrite the inverse resolvent operator as

$$\tilde{\mathcal{R}}^{-1} = -J_z \sum_{j=1}^{6} (S_j^z - s)(S_{j+1}^z - s) - 2J_z s \sum_{j=1}^{6} (S_j^z - s), \tag{71}$$

where the indices are defined as mod 6, so that $S_{6+1}^z=S_1^z$. From this point on, all index arithmetic is defined as mod 6 as well for ease of presentation.

To further simplify the resolvent, we introduce $n_j(\ell,\{q_n\})$ as the number of times the link $(j,j-1)$ has had spin transfer occur on it up to stage ℓ in the process described by the string $\{q_n\}$. Then, by definition, the total number of spin transfer operations is $\Sigma_{j=1}^6 n_j(\ell,\{q_n\})=\ell$. In what follows, we will show that the resolvent can be described only by these six numbers. To see this, notice first that, regardless of the order of spin transfer operations, a spin transfer operator on the link $(j,j-1)$ changes $(S_j^z-s)\to(S_j^z-s-1)$ and $(S_{j-1}^z-s)\to(S_{j-1}^z-s-1)$. Note also that, in the initial state, all $(S_j^z-s)=0$. Thus, at every stage of any process, $(S_j^z-s)=-[n_j(\ell,\{q_n\})+n_{j+1}(\ell,\{q_n\})]$. Using these variables, one can then rewrite the resolvent as

$$\tilde{\mathcal{R}}_\ell^{-1}(\{q_n\}) = 4J_z s\ell - J_z \sum_{j=1}^{6} (n_j^2 + 2n_j n_{j+1} + n_j n_{j+2}), \tag{72}$$

where we have suppressed the explicit dependence of the n_j numbers on $\ell,\{q_n\}$ for clarity. It is more convenient to derive a recursion relation for the resolvent at stage ℓ as follow:

$$\tilde{\mathcal{R}}_{\ell+1}^{-1}(\{q_n\}) = \tilde{\mathcal{R}}_\ell^{-1}(\{q_n\}) + J_z(4s - 1 - 2n_i - 2n_{i+1} - 2n_{i-1} - n_{i+2} - n_{i-2}), \tag{73}$$

where i is the link numbering corresponding to the link acted on at the $\ell+1$ step, $q_{\ell+1}=(i,i-1)$. The initial condition for this recursive series is $\tilde{\mathcal{R}}_0^{-1}=0$. Using Eq. (73), we can calculate the product $\Pi_{\ell=1}^{6s-1}\tilde{\mathcal{R}}_\ell(\{q_n\})$ for a given process. For every process, we need to keep track of only the six numbers n_j in the various steps of the process.

We have calculated the coefficient K explicitly for a number of interesting values of s. The results are summarized in Table II.

IV. LARGE-s EXPANSION

A large-s analysis has recently been employed in Ref. 26 to explore the magnetic order for the general spin-s Heisen-

TABLE II. Values K of the coefficient for the lowest order off-diagonal term for various values of s.

s	K
$\frac{1}{2}$	$\frac{3}{2}$
1	0.884025
$\frac{3}{2}$	0.250931
2	0.0563749
$\frac{5}{2}$	0.0110694
3	0.00199964

berg AFM on the pyrochlore lattice. Restricting the Hilbert space to collinear spin configurations, the authors of Ref. 26 derived an effective Hamiltonian out of the harmonic spin-wave energy contribution to order $\mathcal{O}(s)$. The effective Hamiltonian prefers spin products around hexagonal plaquettes to be $-s^6$ in the zero magnetic field and $+s^6$ in the half-polarized plateau region. Following a terminology inspired by the Ising gauge theory, these are denoted by "π flux" configurations and "zero-flux" configurations, respectively. In order to compare this approach, which is justified in the large-s limit, with the DPT analysis of Sec. III, we have repeated the same type of effective Hamiltonian calculation for the XXZ model. Our derivation closely follows that of Ref. 26.

The large-s expansion consists of expressing the spin degrees of freedom in terms of Holstein-Primakoff bosons and expanding in decreasing powers of s. The lowest-order term in the large-s expansion is of order s^2 and corresponds to the classical spin version of the quantum XXZ Hamiltonian,

$$\mathcal{H}_{\rm cl} = J_z \sum_{\langle ij \rangle} [\alpha(\mathbf{S}_i \cdot \mathbf{S}_j) + (1-\alpha)(\mathbf{S}_i \cdot \hat{z})(\mathbf{S}_j \cdot \hat{z})] - 2J_z h \sum_j S_j^z, \tag{74}$$

where $\alpha = J_\perp / J_z$ as before.

In order to analyze the ground state of this anisotropic classical model (74), we first calculate the minimum energy configuration for a *single* tetrahedron. For the single tetrahedron, we obtain the magnetization curve shown in Fig. 8. We find that for $\alpha < 1$, a half-polarization plateau opens up, and the plateau becomes wider as α decreases from 1. In this plateau, the classical spins on the single tetrahedron being analyzed are in a collinear configuration, with three $\mathbf{S}_j = s\hat{z}$ and one $\mathbf{S}_j = -s\hat{z}$ spins. This is just the classical analog of the 3:1 configuration on a single tetrahedron found in Sec. II. A 3:1 spin configuration can be realized on each and every tetrahedron of the lattice simultaneously. We therefore conclude that in the range of magnetic fields where the single tetrahedron is in a half-polarized state, the ground state of the many-body system (74) is the manifold of 3:1 configurations. This means that the plateaus in the classical XXZ model on the complete pyrochlore lattice are at least as wide as in Fig. 8.

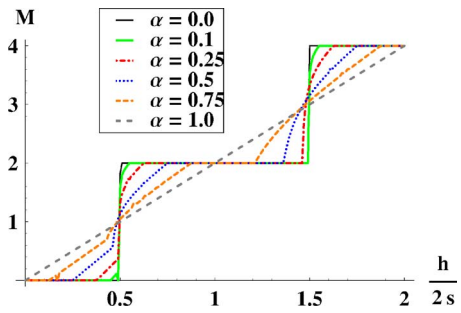

FIG. 8. (Color online) Magnetization (in units of s) of a single tetrahedron of classical spins with an anisotropic XXZ interaction, parametrized by α. For any $\alpha < 1$, a half-polarization plateau exists.

In the following, we will discuss only this half magnetization plateau. We then assume the collinear 3:1 states, which allows us to describe the magnetic configuration in terms of the same Ising variables $\sigma_j = \pm 1$ as in Sec. II.

As in Ref. 26, we use the unitary transformation (17) so that we can define the Holstein-Primakoff bosons, which amounts to replacing the rotated spin operators as follows:

$$S_j^z = s - \hat{m}_j,$$

$$S_j^+ = \sqrt{2s - \hat{m}_j}\,\hat{b}_j \approx \sqrt{2s}\,\hat{b}_j, \tag{75}$$

where $\hat{b}_j$ are canonical bosonic operators and $\hat{m}_j = \hat{b}_j^\dagger \hat{b}_j$ is the boson number operator. We plug these into the Hamiltonian (4) and keep only the quadratic terms in the bosonic operators.

Since the spin configurations are now restricted to the 3:1 manifold, the magnetic-field term is the same for every 3:1 configuration as the magnetization is constant on the plateau. In terms of the *unrotated* spin variables S_j^z, this amounts to $\Sigma_j S_j^z = (s/2)N$, where N is the number of sites in the pyrochlore lattice. Varying the magnetic field in the plateau region causes an overall shift in the spin-wave energies of all the 3:1 states and, thus, will not alter the energy differences between different 3:1 states. Similarly, the Ising variables have a sum of $\Sigma_j \sigma_j = \frac{1}{2}N$, and we can use these two identities to derive $\Sigma_j \sigma_j \hat{m}_j = 0$, which is useful in simplifying other terms. Therefore, we can ignore the magnetic-field term, since we are searching for an effective Hamiltonian splitting the energies of different 3:1 states. The effect of the magnetic field is to determine the energy gap for spin-wave excitations. The vanishing of the spin-wave gap signifies an instability of the 3:1 manifold, corresponding to the edges of the half-polarization plateau.

From Eqs. (B3) and (23), the resulting harmonic spin-wave term reads

$$\mathcal{H}_{\rm harm}^{3:1} = J_z \frac{\alpha}{2} s \sum_{i,j} \Gamma_{ij} \left[\left(\frac{1+\sigma_i\sigma_j}{2} \right) (\hat{b}_j^\dagger \hat{b}_i + \text{H.c.}) + \left(\frac{1-\sigma_i\sigma_j}{2} \right) \times (\hat{b}_j \hat{b}_i + \text{H.c.}) \right] + J_z 2s \sum_j \hat{m}_j. \tag{76}$$

Following the derivation Ref. 26, the zero-point energy of this harmonic term for a given 3:1 spin configuration (described by $\{\sigma_j\}_{j=1}^N$) is

$$E_{\text{harm}} = J_z s \sum_{k=1}^{N} \frac{|\lambda_k|}{2}, \tag{77}$$

where λ_k are the solutions of the eigenvalue equation

$$\left(\frac{\lambda}{2}\right)^2 \mathbf{v} = \left[\mathbf{1} + \frac{\alpha}{2}(\hat{\sigma}\hat{\Gamma}\hat{\sigma} + \hat{\Gamma}) + \left(\frac{\alpha}{2}\hat{\sigma}\hat{\Gamma}\right)^2\right] \cdot \mathbf{v}. \tag{78}$$

In the right-hand side, $\hat{\Gamma}$ denotes the same $N \times N$ connectivity matrix introduced in Sec. II, and $\hat{\sigma}$ is a diagonal $N \times N$ matrix with σ_j as its diagonal elements. Without specifying the 3:1 configuration, we can write an expression for the harmonic energy in terms of σ_j as follows:

$$E_{\text{harm}} = J_z s \, \text{Tr}\left[\sqrt{\mathbf{1} + \frac{\alpha}{2}(\hat{\sigma}\hat{\Gamma}\hat{\sigma} + \hat{\Gamma}) + \frac{\alpha^2}{4}(\hat{\sigma}\hat{\Gamma})^2}\right]. \tag{79}$$

One can calculate the spin-wave energies by assuming a particular spin configuration and computing the trace exactly. However, as in Ref. 26, if one does not know which candidate spin configurations to consider, one can derive an effective Hamiltonian to determine which spin configuration gives the lowest harmonic energy and find a favorable spin configuration.

The square root in Eq. (79) can be expanded in powers of matrix operators. We first observe that α only appears as a multiplier of the matrix Γ. Therefore, an expansion in powers of matrix operators is *equivalent* to expansion in the parameter α. In the present context, this expansion is justified due to the easy-axis anisotropy $\alpha < 1$.

The terms in the expansion can be organized as a sum of traces over products of Γ matrices and the Ising variables σ_j. The order of α for each term also specifies the number of connectivity matrices Γ appearing in that term.

Due to the trace operation, the product of Γ matrices represents closed loops on the lattice. The Ising variables appearing in each such term can only involve the sites on the loops defined by the product of Γ matrices. Using the results of Sec. III B 2, which discuss functions of the Ising variables and Γ matrices precisely of the form appearing in this expansion, it is evident that all terms involving less than six Γ matrices will result in constants, which will not split energies of the 3:1 states. As in Sec. II, the lowest-order term in the expansion in α causing energy splitting in the 3:1 manifold involves loops around hexagonal plaquettes of the pyrochlore lattice. For simplicity, we consider only these terms and ignore any higher-order term in the expansion in α. After extensive simplification, the sixth-order term reads

$$\begin{aligned}\mathcal{H}_{\text{harm}} = J_z s \left(\frac{\alpha}{2}\right)^6 \frac{1}{512} [&14\,\text{Tr}(\sigma\cdot\Gamma\cdot\sigma\cdot\Gamma^5) \\ &+ 14\,\text{Tr}(\sigma\cdot\Gamma^2\cdot\sigma\cdot\Gamma^4) + 7\,\text{Tr}(\sigma\cdot\Gamma^3\cdot\sigma\cdot\Gamma^3) \\ &- 6\,\text{Tr}(\sigma\cdot\Gamma\cdot\sigma\cdot\Gamma\cdot\sigma\cdot\Gamma\cdot\sigma\cdot\Gamma^3) \\ &- 3\,\text{Tr}(\sigma\cdot\Gamma^2\cdot\sigma\cdot\Gamma\cdot\sigma\cdot\Gamma^2\cdot\sigma\cdot\Gamma) \\ &- 6\,\text{Tr}(\sigma\cdot\Gamma^2\cdot\sigma\cdot\Gamma^2\cdot\sigma\cdot\Gamma\cdot\sigma\cdot\Gamma) \\ &+ \text{Tr}(\sigma\cdot\Gamma\cdot\sigma\cdot\Gamma\cdot\sigma\cdot\Gamma\cdot\sigma\cdot\Gamma\cdot\sigma\cdot\Gamma\cdot\sigma\cdot\Gamma)] \\ &+ O(\alpha^8).\end{aligned} \tag{80}$$

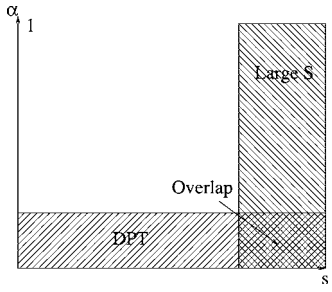

FIG. 9. This figure shows the regions of parameter space where the DPT and large-S expansions are justified and their region of overlapping validity.

From the expression, one extracts only those terms corresponding to loops around hexagonal plaquettes. Equation (80) takes the form of the function in Eq. (39), with $n=6$ and the "loop" diagram $G_n = \{(12),(23),(34),(45),(56),(61)\}$. The corresponding function $f(\sigma_{a_1},\ldots,\sigma_{a_6})$ reads

$$\begin{aligned}f(\sigma_{a_1},\ldots,\sigma_{a_6}) = &\,14\sigma_{a_1}\sigma_{a_2} + 14\sigma_{a_1}\sigma_{a_3} + 7\sigma_{a_1}\sigma_{a_4} \\ &- 6\sigma_{a_1}\sigma_{a_2}\sigma_{a_3}\sigma_{a_4} - 3\sigma_{a_1}\sigma_{a_3}\sigma_{a_4}\sigma_{a_6} \\ &- 6\sigma_{a_1}\sigma_{a_3}\sigma_{a_5}\sigma_{a_6} + \sigma_{a_1}\sigma_{a_2}\sigma_{a_3}\sigma_{a_4}\sigma_{a_5}\sigma_{a_6}.\end{aligned} \tag{81}$$

The effective Hamiltonian therefore describes all possible spin interactions on the hexagonal plaquette of the pyrochlore lattice—two, four, and six spin interactions. It is far more convenient to express this complicated Hamiltonian in terms of energies of plaquette configurations, in the same way we formulated the results of the DPT in Sec. II as $\mathcal{H}_{\text{harm}} = \Sigma_P \mathcal{E}_P$ (using the same five plaquettes in Table I).

As in Sec. III C, there are only three independent plaquette configuration energies $V_{1,2,4}$, which to $O(\alpha^6)$ are

$$V_1 = 0,$$

$$V_2 = \frac{J_z \alpha^6 s}{512},$$

$$V_4 = 0. \tag{82}$$

Comparing Eq. (82) with Eq. (64), we find complete agreement between the DPT of Sec. II and the large-s expansion of this section in the limit of both $\alpha \to 0$ and $s \to \infty$, where both approaches are justified (see Fig. 9). This serves an excellent check on the correctness as well as validity of our calculations in the parameter regime where the approximations overlap.

V. LOW-ENERGY STATES OF THE EFFECTIVE HAMILTONIAN

A. Strict easy-axis limit for $s \geqslant 3/2$

In this section, we consider the $\alpha = J_\perp / J_z \ll 1$ limit, for which the lowest-order nonvanishing terms in the effective Hamiltonian are dominant. For any $s \geqslant 3/2$, this is just the sixth-order diagonal contribution.

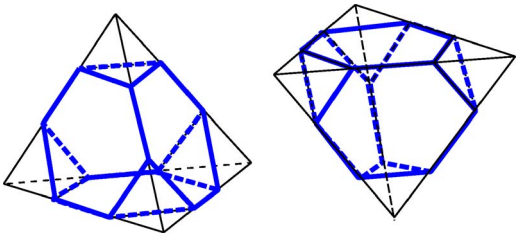

FIG. 10. (Color online) A cell is composed of four link-sharing hexagonal plaquettes [the polyhedron bounded by thick (blue) lines]. The cell on the left is up-headed and the one on the right is a down-headed cell.

1. Infinite s case

We first consider the infinite s limit. As is clear from Eq. (82) that at order s, only the type 2 plaquette suffers from a *positive* energy correction, while V_1 and V_4 are only nonzero at order s^0 or lower. Hence, the type 2 plaquette is strongly disfavored for large s in general and completely disallowed for infinite s. This in combination with the 3:1 constraint allows us to restrict ourselves to the "0-flux manifold" in the large-s region (see Sec. IV for the definition of a 0-flux manifold.).

To see this, let us first introduce a "cell" comprised by four link-sharing plaquettes. Choose four hexagonal plaquettes such that any pair of two plaquettes out of these four plaquettes always shares a link. Then, these four plaquettes form a single polyhedron (a truncated tetrahedron), with four hexagonal faces and four triangular faces (see Fig. 10). We will refer to this polyhedron as a cell. In the pyrochlore lattice, one may distinguish two kinds of cells—when one completes the tetrahedra enclosing a cell, we can identify *up-headed* and *down-headed* cells, according to the direction at which the tetrahedra are pointing (see Fig. 10 for examples of both kinds). Each up- and/or down-headed cell shares its faces (hexagonal plaquettes) with four nearest-neighboring down- and/or up-headed cells. Thus, centers of cells constitute a diamond lattice, where those of up-headed cells take part of one fcc lattice and those of down-headed cells form the other fcc lattice. The up-headed cells contain all the up-pointing tetrahedra, and so it suffices to determine the spin configuration on only these up-headed (down-headed) cells in order to specify the spin configuration on all sites of the lattice.

Observing the local constraint, one can readily enumerate the various minority-spin configurations of a cell. In Table III, all possible cell configurations allowed in the 3:1 manifold are listed. Each cell type is described by the configurations of its four hexagonal plaquettes.

To see that the ground-state manifold in the large-s region is composed only of type 0, 3, and 4 plaquettes (i.e., 0-flux states), notice from Table III that any cell type which contains a type 1 plaquette always contains at least one type 2 hexagonal plaquette. This implies

$$0 \leqslant x_1 \leqslant x_2, \tag{83}$$

where x_a are the plaquette-type fractions, as introduced in Sec. III C. Disallowing the type 2 plaquette inevitably leads to excluding the type 1 plaquette, and, therefore, the positive V_2 in leading order of s^{-1} expansion allows us to conclude that the classical ground-state spin configurations in the infinite s limit consist of only the 0-flux states.

TABLE III. The various cell configurations are described by the number of each plaquette type included in the plaquettes comprising a cell. In the zero-flux manifold, only types 9, 10, 11, and 12 cells are allowed, since they do not contain types 1 and 2 hexagonal plaquettes. Furthermore, a cell must contain a type 2 plaquette whenever it contains a type 1 plaquette. This is quantified by $0 \leqslant x_1 \leqslant x_2$.

	Plaquette				
Cell	Type 1	Type 2	Type 3	Type 4	Type 0
Type 1	1	1	1	1	0
Type 2	1	3	0	0	0
Type 3	0	4	0	0	0
Type 4	0	2	2	0	0
Type 5	0	2	1	1	0
Type 6	0	2	1	0	1
Type 7	0	2	0	1	1
Type 8	0	2	0	0	2
Type 9	0	0	4	0	0
Type 10	0	0	2	1	1
Type 11	0	0	0	3	1
Type 12	0	0	0	0	4

2. Large-s case

Next, we turn to consider the large but finite s limit. The ground states of the infinite s limit, the 0-flux states, are massively degenerate. However, higher-order quantum corrections in s^{-1} can select a particular classical state out of this 0-flux manifold. To see this, let us expand the plaquette energies in s^{-1},

$$\frac{V_1}{J_z\alpha^6} = -\frac{3}{512} + O(s^{-1}),$$

$$\frac{V_2}{J_z\alpha^6} = \frac{s}{512} + \frac{3}{1024} + O(s^{-1}),$$

$$\frac{V_4}{J_z\alpha^6} = \frac{17}{65\,536s} + O(s^{-2}). \tag{84}$$

Notice first that the $\mathcal{O}(1)$ negative energy correction to V_1 plays no role in lifting the degeneracy of the 0-flux manifold, since this manifold does not contain any type 1 hexagonal plaquettes. Thus, provided that V_2 dominates the other two, the most relevant correction in the large-s limit is V_4, which always disfavors the type 4 hexagonal plaquette, since it is positive.

Since the type 4 plaquette is disfavored, observing the 0-flux condition on all plaquettes, we have only to minimize x_4 to obtain the ground state in the large-s region. However,

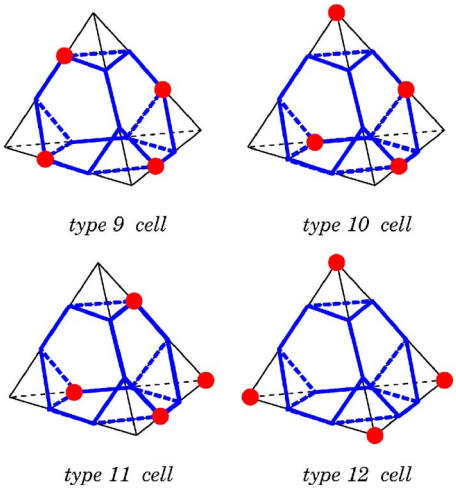

FIG. 11. (Color online) The four cell types allowed in the zero-flux manifold. Minority sites are specified by the (red) circles.

in the 3:1 manifold, the 0-flux condition becomes so strong that x_4 is, in fact, bounded by $\frac{3}{28}$ from below $\left(x_4 \geqslant \frac{3}{28}\right)$. To see this, notice first that only types 9, 10, 11, and 12 cells drawn in Fig. 11 are allowed in the 0-flux manifold. Next, we denote by $y_{9,10,11,12}$ the fraction of cell types 9,…,12 in the entire pyrochlore lattice [we use these instead of plaquette-type fractions (x_3, x_4, x_0) for later convenience]. In the 0-flux manifold, only these cell types may occur, and therefore $\Sigma_{j=9}^{12} y_j = 1$. Together with the "global" 3:1 constraint, i.e., Eq. (57), one finds

$$3y_{12} = y_9, \tag{85}$$

as well as

$$y_{12} = \frac{1}{4}(1 - y_{10} - y_{11}). \tag{86}$$

An important step to identify the lower bound on x_4 is to note that packing these four cell types into a pyrochlore lattice is highly constrained by the *local* 3:1 rule imposed on each tetrahedron. We shall note three useful facts in particular:

(i) A type 12 cell can only have cell types 10, 11, and 12 as neighboring cells.

(ii) Each type 10 and 11 cell can neighbor at most one type 12 cell, as they both have only one type 0 plaquette, and the type 12 cell consists only of type 0 plaquettes.

(iii) One can show that a type 12 cell can have at most one neighboring type 12 cell, and the remaining neighboring cells must be of type 10 or 11.

As a result of (i), (ii), and (iii), we find that a type 12 cell, if it neighbors no other type 12 cell, mandates four other cells to be type 10 or 11. Otherwise, if we have two adjacent type 12 cells, all the other cells adjacent to them must be of type 10 or 11. In this latter case, the two type 12 cells mandate six other cells to be type 10 or 11. We conclude from this short analysis that each type 12 cell mandates the existence of at least three cells of type 10 or 11 and that these

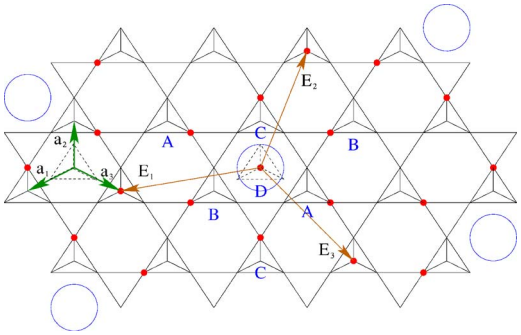

FIG. 12. (Color online) The trigonal$_7$ state. The spin configuration of a planar layer of tetrahedra is shown. Triangles with lines connected at their centers represent up-pointing tetrahedra, while the other triangles represent down-pointing tetrahedra. Minority sites are denoted by small solid circles (red). Two dashed triangles denote up-pointing tetrahedra in the planar layer of tetrahedra immediately above the one depicted in this figure. These two tetrahedra are used to show the primitive vectors for the pyrochlore lattice $\mathbf{a}_{1,2,3}$ and for the magnetic unit cell of the trigonal$_7$ state $\mathbf{E}_{1,2,3}$. The seven up-pointing tetrahedra included in one valid choice of a magnetic unit cell for the trigonal$_7$ state are marked by (blue) letters, indicating one of 4 3:1 configurations for a single tetrahedron. The type 0 plaquettes residing between pairs of adjacent type 12 cells are marked by large open circles (blue).

cells *cannot* be shared by other type 12 cells [see (ii)]. The total number of type 10 and 11 cells must therefore exceed the number of type 12 cells threefold, or in terms of the cell type fractions

$$3y_{12} \leqslant y_{10} + y_{11}. \tag{87}$$

Now, using Eq. (86), we obtain the lower bound on the fraction of type 10 and 11 cells: $y_{10} + y_{11} \geqslant \frac{3}{7}$. Since these two types of cell are the only cells allowed in the 0-flux manifold, which have type 4 hexagonal plaquettes, this lower bound immediately gives us that for the fraction of type 4 hexagonal plaquette,

$$x_4 = \frac{1}{4}y_{10} + \frac{3}{4}y_{11} \geqslant \frac{1}{4}y_{10} + \frac{1}{4}y_{11} \geqslant \frac{3}{28}. \tag{88}$$

From the derivation in Eq. (88), one can easily see that the equal sign can be realized only if $y_{11}=0$. Excluding type 11 cell configurations $y_{11}=0$, the bound becomes $y_{10} \geqslant \frac{3}{7}$. Saturating the bound with $y_{10}=\frac{3}{7}$ determines completely the ratios of the cell types, via Eqs. (85) and (86), to be $y_9 : y_{10} : y_{11} : y_{12} = 3:3:0:1$ (or equivalently, $x_0 : x_1 : x_2 : x_3 : x_4 = 7:0:0:18:3$).

With the type 11 cells excluded, one can show that any type 12 cell *always* neighbors three type 10 cells and one type 12 cell. As a consequence, the condition $3y_{12}=y_{10}$ is satisfied only when any type 10 cell has a type 12 cell as its nearest-neighboring cell, through its single type 0 plaquette.

In what follows, we will show that this lower bound for x_4 is *uniquely* (up to a finite degeneracy) realized by the *periodic* minority-spin configuration depicted in Fig. 12. This collinear magnetic ordered state, which we shall refer to as the "trigonal$_7$" state, contains seven pyrochlore unit cells in

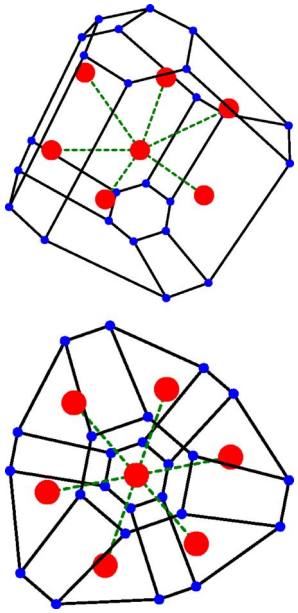

FIG. 13. (Color online) Wigner-Seitz cell of the trigonal$_7$ state. Large solid (red) circles denote the basis positions (the minority sites in the trigonal$_7$ state). The solid lines denote the edges of the Wigner-Seitz cell, and the small solid (blue) circles denote the corners of this cell. The dashed (green) lines are used as a guide to the eyes for the relative positions of the basis points.

the magnetic unit cell. The magnetic ordering has primitive vectors $\mathbf{E}_1=2\mathbf{a}_1-\mathbf{a}_3$, $\mathbf{E}_2=2\mathbf{a}_2-\mathbf{a}_1$, and $\mathbf{E}_3=2\mathbf{a}_3-\mathbf{a}_2$, where $\mathbf{a}_{1,2,3}$ are the primitive unit vectors of the pyrochlore lattice [fcc lattice vectors $\mathbf{a}_1=a/2(0,1,1)$ and cyclic permutations]. From the unit-cell vectors, we can find the volume of the magnetic unit cell as follows:

$$(\mathbf{E}_1\times\mathbf{E}_2)\cdot\mathbf{E}_3=7(\mathbf{a}_1\times\mathbf{a}_2)\cdot\mathbf{a}_3. \tag{89}$$

These three primitive vectors are of equal lengths and are not mutually perpendicular. Therefore, the magnetic Bravais lattice is in the *trigonal* crystal system—-whence the name trigonal$_7$ state. In Fig. 13, we show the Wigner-Seitz cell of a lattice with primitive vectors $\mathbf{E}_{1,2,3}$, together with a basis of the minority sites only.

From the planar view in Fig. 12, it is clear that this magnetic state has a threefold rotation symmetry about the $\mathbf{a}_1+\mathbf{a}_2+\mathbf{a}_3=a(1,1,1)$ axis perpendicular to the page. In the direction of the pyrochlore lattice primitive Bravais vectors, there is a periodicity of 7, giving rise to a sevenfold degeneracy due to fcc lattice translations alone. The trigonal$_7$ state breaks a reflection symmetry about a plane perpendicular to the Kagome plane, parallel to a_2, and passing through the point where the three vectors $\mathbf{E}_{1,2,3}$ originate in the figure (see Fig. 14 for another view of this symmetry operation). Together with the fourfold choice of the set of Kagome planes, it is evident that the degeneracy of this magnetic state is $4\times7\times2=56$.

As is clear from Fig. 12, the spin configuration satisfies both the local zero-flux condition and the local 3:1 constraint. Counting the fractions of plaquette types, we find that the trigonal$_7$ state realizes the lower bound $x_4=\frac{3}{28}$. We conclude that the trigonal$_7$ state is *at least* one of the ground states in the large-s region.

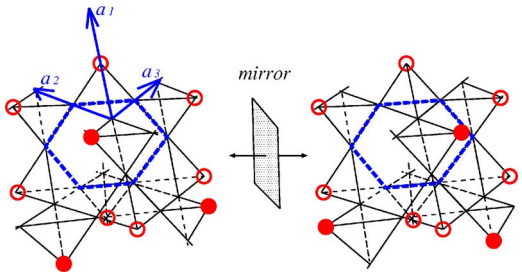

FIG. 14. (Color online) The broken reflection symmetry. Starting from a type 12 (up-headed) cell, and drawing the ten tetrahedra surrounding it, we first choose the place of the nearest-neighboring type 12 cell (down-headed)—the two type 12 cells share the hexagonal plaquette marked by thick dashed (blue) lines. With this choice, the minority sites on seven tetrahedra are automatically determined [marked by open (red) circles]. However, minority sites for the other three tetrahedra [solid (red) circles] are not fully determined and we still have a "mirror" degree of freedom. For convenience, we also draw the primitive vectors of pyrochlore lattice, in accordance with those defined in Fig. 12.

As argued above, any state saturating the bound must have every type 0 plaquette connecting between a type 12 cell and a type 10 cell. We shall refer to this as the cell composition rule. Starting with a type 12 cell and using this rule together with the 3:1 constraint and the zero-flux condition suffice to uniquely construct the trigonal$_7$ state up to the finite degeneracy described above. Starting from the initial type 12 cell, the plaquette connecting this cell to another type 12 cell defines the Kagome plane in Fig. 12. Next, pick one of the two mirror image choices in Fig. 14 of the type 10 cell configurations neighboring the first type 12 cell. From this point on, the three rules mentioned above (the cell composition rule, the 3:1 constraint, and the zero-flux condition) uniquely determine the rest of the magnetic configuration in the entire lattice.

Finally, the energy per plaquette of the trigonal$_7$ state is

$$\frac{1}{N}E_{\text{trigonal}_7}=\frac{3}{28}V_4. \tag{90}$$

3. Spin $s\geqslant 2$

We expect that the trigonal$_7$ state described above is the ground state for sufficiently large s. In the following, we shall argue that this is indeed the case for $s\geqslant 2$. For $s=3,5/2,2,3/2,1$, the energy parameters in the effective Hamiltonian are given in Table IV.

For all the cases in Table IV, V_1 is the largest and most negative energy. This would suggest that the lowest-energy 3:1 state is the one with a maximum number of plaquettes of type 1. However, the geometry of the lattice as well as the 3:1 constraint pose stringent restrictions. From the inequality (83) we previously derived, we see that the energy of a type 1 plaquette is offset by the energy cost of a type 2 plaquette, which is the *highest-energy* cost for all the s values in Table IV. Therefore, the number of type 1 plaquettes is not neces-

TABLE IV. Energies $V_{1,2,4}$ of the plaquette configurations types 1, 2, and 4 for $s=3, \frac{5}{2}, 2, \frac{3}{2}, 1$.

Energy	$s=3$	$s=\frac{5}{2}$	$s=2$	$s=\frac{3}{2}$	$s=1$
$\frac{V_1}{J_z\alpha^6}$	−0.0100	−0.0113	−0.0135	−0.0188	−0.0410
$\frac{V_2}{J_z\alpha^6}$	0.0097	0.0090	0.0084	0.0083	0.0099
$\frac{V_4}{J_z\alpha^6}$	0.0001	0.0002	0.0003	0.0005	0.0015
K	0.0020	0.0111	0.0564	0.2509	0.8840

sarily maximized in the ground state even with small s. Because of this, V_2 is significant, despite its small magnitude. In contrast, due to its very small magnitude compared with both $V_{1,2}$, V_4 will not play a significant role in determining the energetically favored states.

One observes that the magnitude of the energy V_1 is comparable to V_2 already at $s=5/2$, and this trend continues to higher s—V_2 becomes more dominant. Given the restriction $x_1 \leqslant x_2$ and the large energy cost of type 2 plaquettes, it may be that for $s \geqslant 5/2$, type 2 plaquettes are excluded completely, just as in the above subsection, and then the trigonal$_7$ state may be the lowest-energy state for $s \geqslant 5/2$. The case $s=2$ is close to the boundary for a change in behavior.

In order to search for other candidate ground states, we have enumerated all 3:1 states on a variety of periodic finite clusters and determined the exact lowest-energy state for each one for $s=1,3/2,2,5/2,\cdots,6$. For $s \geqslant 2$, we find no states with lower energy than that of the trigonal$_7$ state. This strongly suggests that the trigonal$_7$ state is the ground state for all $s \geqslant 2$, though of course this limited numerical investigation does not constitute a proof that this is the case. Moreover, states with large numbers of type 1 plaquettes are among the highest-energy states we have found, which does give credence to our assessment that when the V_2 and V_1 are comparable energy scales (with opposite signs); because of the condition $x_1 \leqslant x_2$, the energy V_2 is still dominant. One can conclude that *if* there is a state with lower energy for $s \geqslant 2$, it must have a large unit cell, which is incompatible with all the clusters considered in Table V.

4. Spin s=3/2

Spin $s=3/2$ is the smallest spin value for which in the extreme easy-axis limit $\alpha \ll 1$, the off-diagonal term in the effective Hamiltonian may be ignored. The corresponding plaquette energies are given in column 4 of Table IV. The energy for type 1 plaquettes is approximately 50% larger (more negative) than for $s=2$. In the extreme limit of very large and negative V_1, the ground state has been determined previously in Ref. 9. The state, referred to as the **R** state in Ref. 9 as well as in the remainder of this paper, maximizes the fraction of type 1 plaquettes and is unique (up to lattice symmetries).

The numerical investigation mentioned in the previous section shows that the **R** state is not the lowest-energy state

TABLE V. 3:1 configurations on periodic clusters. Energy is given in units of $J_z\alpha^6$.

		$s=\frac{3}{2}$	
Number of unit cells	Number of 3:1 states	E	gs
$2\times2\times1=4$	36	1.3×10^{-4}	4
$2\times2\times2=8$	272	1.3×10^{-4}	12
$4\times2\times1=8$	708	1.3×10^{-4}	4
$3\times3\times1=9$	1,120	-2.9×10^{-4}	24
$5\times2\times1=10$	3,370	4×10^{-4}	4
$3\times2\times2=12$	2,436	1.3×10^{-4}	4
$4\times2\times2=16$	23,696	1.3×10^{-4}	12
$6\times3\times1=18$	649,480	-2.9×10^{-4}	192
$3\times3\times2=18$	61,192	-2.9×10^{-4}	30
$5\times2\times2=20$	237,156	1.3×10^{-4}	4
$4\times3\times2=24$	1,685,508	1.3×10^{-4}	4
$3\times3\times3=27$	7,515,136	-2.9×10^{-4}	216

for the diagonal effective Hamiltonian at $s=3/2$. Instead, we find a highly degenerate set of classical ground states. One example of these states has all the minority sites contained in a set of parallel Kagome layers of the pyrochlore lattice. Every Kagome plane can have the configuration shown in Fig. 15, or two other symmetry related configurations with the same $\sqrt{3}\times\sqrt{3}$ structure in the Kagome planes, *independent* of the other Kagome planes. We shall refer to this large subset of this manifold of states as the $\sqrt{3}\times\sqrt{3}$ states.

The analysis of this degenerate manifold of states is somewhat involved. We therefore leave the details to Appendix C and only mention a number of facts here. All the states we have found numerically have plaquette-type fractions of $x_0=1/6, x_1=1/6, x_2=1/3, x_3=1/6$, and $x_4=1/6$. As a consequence, the energy per plaquette of these states is

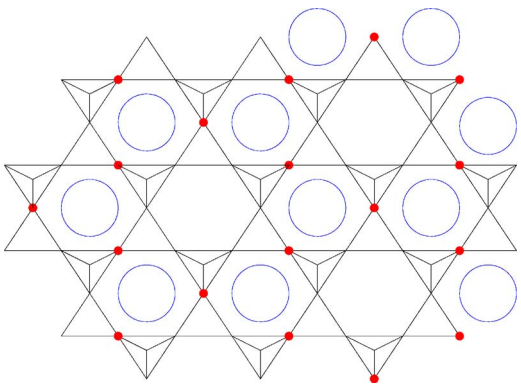

FIG. 15. (Color online) 3:1 spin configuration of a single layer of tetrahedra in the $\sqrt{3}\times\sqrt{3}$ state. Only minority-spin sites are marked by (red) solid circles. Flippable plaquettes (type 1) are denoted by an open (blue) circle drawn at their center. The same conventions as in Fig. 12 are used here.

$$\frac{1}{N}E_{\sqrt{3}\times\sqrt{3}} = \frac{1}{6}(V_1 + 2V_2 + V_4). \tag{91}$$

In Appendix C, we show by explicit construction that the degeneracy is at least

$$18 \times 2^{N/12L} + 4 \times 3^L - 36, \tag{92}$$

which grows exponentially with system size. We have not shown that the above states exhaust the possibilities with energy given by Eq. (91), so the above formula is only a lower bound for the degeneracy.

B. Effect of off-diagonal term

In this section, we add to the effective Hamiltonian the off-diagonal term where it is likely to be important (low values of s). For $s=1/2$, the off-diagonal term is parametrically larger than the diagonal terms in the $\alpha \ll 1$ limit. For $s=1$, it is of the same order as the diagonal terms. However, in this case, the off-diagonal term is numerically more than 20 times bigger than the largest diagonal plaquette energy and should therefore dominate. For $s \geqslant 3/2$, the off-diagonal term is negligible in the $\alpha \ll 1$ limit, but extrapolating the DPT results to the isotropic case $\alpha=1$, the off-diagonal term may be significant and, in some cases, may even be dominant.

Comparing the diagonal energy scales and K in Table IV, we find that for spin $s=3/2$, the off-diagonal term dominates in the isotropic ($\alpha=1$) limit. For spin $s=2,5/2$, the diagonal energy scales are significant compared with K.

For spin $s=3$, K is smaller than the diagonal energy scales. From Table II, we can see that K decreases rapidly as s increases. The form of K in Eq. (70) would suggest that the decay is a result of the factor $1/2^{6s}$. The off-diagonal term is not accessible in the perturbative large-s expansion and, therefore, must be exponentially decaying in s. Examining the values in Table II, we find that indeed K decreases exponentially with s. In contrast, the diagonal energies change far slower, as is evident at large s from Eq. (84). The off-diagonal term then becomes less important for higher spin values.

We therefore conclude that when extrapolating to $\alpha=1$, for spin $s \geqslant 3$, the diagonal term remains more significant than the off-diagonal term, while for $s \leqslant 3/2$, the diagonal term can most likely be neglected. For $s=2,5/2$, both diagonal and off-diagonal terms may be important.

In what follows, we will discuss several likely phases for different spins in the isotropic limit $\alpha=1$ from the perspective of order by disorder and the general theoretical framework of QDM-type models.

1. Purely off-diagonal QDM: $s \leqslant 3/2$ case

Let us consider first the simple case of $s \leqslant 3/2$, for which the Hamiltonian is approximated by including the off-diagonal only. Clearly, low-energy ground states of this Hamiltonian must have significant amplitude for type 1 plaquettes, as other plaquettes are annihilated by the off-diagonal term. We note that the trigonal state has no type 1 plaquettes. This implies that it is an exact zero energy eigenstate of the purely kinetic Hamiltonian. Since it is straightforward to construct states with significantly negative energy per plaquette, the classical trigonal$_7$ state is clearly an excited state in this case. It seems difficult to imagine any way that the ground state could be adiabatically connected to the trigonal state (or any other zero energy state with no type 1 plaquettes).

Let us instead consider what sort of states might naturally minimize the energy of the kinetic term. This sort of pure QDM problem has been considered in numerous places in the literature. Specifically for the QDM on the diamond lattice, the question has been discussed in Ref. 33 (see references therein for a guide to QDMs). Roughly speaking, the energy is minimized by delocalizing the wave function as much as possible among different dimer configurations. However, the nontrivial connectivity in the constrained space of dimer coverings makes the nature of this delocalization subtle.

One possibility in such a three-dimensional QDM is that the ground state is a U(1) *spin liquid*, in which the delocalization is sufficiently complete as to prevent any symmetry breaking [the meaning of the U(1) is discussed in depth in, e.g., Ref. 2]. Roughly speaking, the wave function has support for all possible dimer coverings, with equal amplitudes for all topologically equivalent configurations. The existence and stability of such a state can be established in a QDM with a particular form of diagonal interaction, in the neighborhood of the so-called Rokhsar-Kivelson (RK) point. While this point (corresponding to $V_1=K>0$, $V_2=V_4=0$) is not physically relevant to the pyrochlore antiferromagnets, it is possible that such a U(1) spin-liquid state remains the ground state for the purely off-diagonal QDM.

A second possibility is that the delocalization is incomplete, due to "order-by-disorder" physics. In particular, it may be favorable to delocalize only over a limited set of classical states, among which the connections are greater than those among generic classical configurations. In this case, there is generally some symmetry breaking induced by the selection of the states involved. Two sorts of such ordering have been proposed and observed in other similar QDM models. The first type of order-by-disorder state is the one in which the set of classical states for which the ground-state wave function has the largest amplitude are "centered" about a single classical state having the maximal number of type 1 plaquettes. Such a wave function may be "selected" by the kinetic energy, since under the action of the kinetic term of the QDM, this is the classical state that is connected to the *largest number* of other classical states. In our problem, this classical state is just the **R** state mentioned above and discussed at length in Refs. 9 and 10. A simple form for such a wave function is

$$|\mathbf{R},\{\gamma_P\}\rangle = \exp\left[\sum_P \gamma_P(|\hexagon\rangle\langle\hexagon| + \text{H.c.})\right]|\mathbf{R}\rangle, \tag{93}$$

where $|\mathbf{R}\rangle$ is the classical **R** state (with definite $S_i^z = S\sigma_i$) and γ_P are variational parameters, which can be used to optimize the quantum state $|\mathbf{R},\{\gamma_P\}\rangle$.

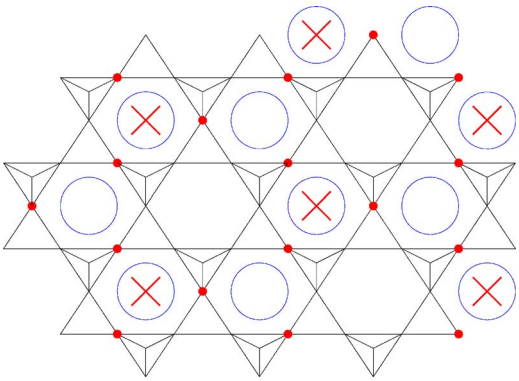

FIG. 16. (Color online) Choice of nonoverlapping flippable plaquettes to resonate in a plane of the $\sqrt{3}\times\sqrt{3}$ state. The chosen plaquettes are marked with (red) crosses in the middle. The minority sites are marked by solid (red) circles.

The second type of order-by-disorder state is the one in which there are a maximal number of *independently resonating plaquettes*. This is based on the observation that the exact ground state for the kinetic term on a single plaquette is simply an equal amplitude superposition of the two type 1 states. However, neighboring plaquettes share sites, and, therefore, it is not possible to form a direct product of such resonances on *all* plaquettes. Instead, the best one can naïvely do along these lines is to find the classical state with the largest number of type 1 plaquettes, which can be *independently flipped*, and on these type 1 plaquettes form an equal amplitude superposition of these two states.

A state with the maximal number of independently flippable plaquettes can be described starting from the $\sqrt{3}\times\sqrt{3}$ states introduced in Sec. V A 4. The largest set of independently flippable plaquettes is a subset of all the type 1 plaquettes. An appropriate choice in a single plane is demonstrated in Fig. 16, which includes half of the flippable plaquettes in the plane. It is interesting to point out that in each plane, there are two possible choices of the plaquettes to be resonated (one half or the other), so out of each $\sqrt{3}\times\sqrt{3}$ state, we can construct 2^L different choices of the plaquettes that will be resonating. The degeneracy of these state is therefore $2^L\times 3^L\times 4=6^L\times 4$. Other states realizing this maximum number of independently resonating plaquettes may be possible, but we have not pursued this further. We refer to these states as "resonating plaquette states" (RPS). A precise wave function describing the RPSs we have derived from the $\sqrt{3}\times\sqrt{3}$ states is

$$|\mathrm{RPS}\rangle = \prod_{P\in G}\frac{1}{\sqrt{2}}(1+(|\hexagon_A\rangle\langle\hexagon_B|+\mathrm{H.c.}))|\Psi\rangle, \qquad (94)$$

where G denotes the set of nonoverlapping resonating plaquettes and $|\Psi\rangle$ denotes one of the $\sqrt{3}\times\sqrt{3}$ states. There are 4×3^L choices for $|\Psi\rangle$ and 2^L choices for G given $|\Psi\rangle$. We note that the *symmetry* of the RPS is distinct and lower than that of the $\sqrt{3}\times\sqrt{3}$ state—even in a single layer. Thus there is a precise distinction between these two states independent of the detailed form of their wave functions, for which the above explicit forms are of course only crude approximations.

While potentially there might be some other state we have not anticipated, we think that most likely one of the three above states obtains in the purely kinetic QDM, which we argue is valid for $s\leqslant 3/2$. We will, however, refrain from making any definite statement as to which of these is the true ground state. One may imagine comparing the energies of the wave functions in Eqs. (93) and (94) to gauge the relative favorability of the **R** and RPS states. Unfortunately, even evaluating the variational energy of the $|\mathbf{R}\rangle$ state in Eq. (93) is rather challenging. Another difficulty is the considerable freedom in choosing the RPS wave functions. Furthermore, a good variational wave function for the spin liquid is also needed for a more complete comparison. As always, there is much arbitrariness in defining each variational wave function, making the predictive power of such an approach unclear. We believe that this issue is more likely to reliably resolved in the future through numerically exact methods such as quantum Monte Carlo or exact diagonalization.

2. $s\geqslant 3$ QDMs

For $s\geqslant 3$, the diagonal term is always larger in energy scale than the off-diagonal term. A crude guess would be to completely neglect the off-diagonal term, in which case the ground state is the trigonal$_7$ state. In all known QDMs, whenever the diagonal term has an energy scale larger than that of the off-diagonal term, the state is determined exclusively by the diagonal term. We therefore presume that it is unlikely that the off-diagonal term is strong enough to change the state of the system and expect the structure of the trigonal$_7$ state to persist for all $s\geqslant 3$.

3. $s=2,5/2$ QDMs

For $s=2,5/2$, the ground state of the classical diagonal term alone is the trigonal$_7$ state, which is strongly disfavored by the kinetic term. In the last paragraph of Sec. V A 3, we mentioned that for $s\geqslant 2$, states with high numbers of type 1 plaquettes are disfavored by the diagonal term. As a result of this observation, we may speculate that the high energetic cost for type 1 plaquettes can be qualitatively captured by a single diagonal energy $V_1>0$.

To get an idea for the energy scale of this effective diagonal term, consider the difference between the diagonal energy per plaquette for trigonal$_7$ and **R** states, which is 2.9×10^{-3} and 3.9×10^{-3} for $s=2,5/2$, respectively. Since these energy differences are smaller than K for $s=2,5/2$, we expect the effective diagonal term to satisfy $0<V_1<K$.

In this effective QDM, we are closer to the RK point $V_1=K>0$ than in the case of the kinetic term alone $V_1=0$. While any of the ground states discussed in Sec. V B 1 may also be the ground state here, the additional diagonal term $V_1>0$ presumably lowers the energy of a U(1) spin-liquid state relative to the RPS and **R** state.

VI. DISCUSSION

Since the development of the DPT and its analysis in this paper are rather involved, we begin in the first Sec. VI A by

recapitulating the central points. In the second Sec. VI B, we will then turn to a brief discussion of the implications on experiments and future directions of this work.

A. Summary

As a prototypical model of a magnetization plateau in a strongly frustrated quantum antiferromagnet, we considered in this paper a nearest-neighbor spin-s model on the pyrochlore lattice at half the saturation magnetization. Such plateaus have been observed in the spinel materials such as $HgCr_2O_4$ and $CdCr_2O_4$. We argued that a useful starting model is the easy-axis XXZ Heisenberg model in an external field, Eq. (4). This model possesses all the same symmetries as the isotropic Heisenberg model in an external field, and indeed we were able to extrapolate our results to this limit. This model has the advantage that the transverse spin fluctuations can be treated systematically as a perturbation to the underlying Ising model. The resulting Ising model can be rewritten as a sum over the elementary tetrahedra of the pyrochlore lattice. In this Ising limit on the plateau, the spins on each tetrahedron satisfy a 3:1 constraint, comprising a set of three majority spins fully polarized parallel to the field and one minority spin antiparallel to the field. The half-polarized state has a macroscopic degeneracy corresponding to the number of possible positions for all the down-pointing spins in the lattice. It is expected that the transverse spin fluctuations will play a role in selecting a ground state or set of ground states from the massively degenerate 3:1 manifold. In this way, we are led to a theoretical model involving a "constrained" degenerate perturbation theory in the 3:1 manifold. Our paper is devoted to a detailed analysis of such a theory and many parts are couched in sufficiently general language to be applicable to a broad class of systems.

We began our discussion of the constrained easy-axis degenerate perturbation theory by deriving the general structure of the effective Hamiltonian that occurs at each order of dimensionless coupling $\alpha=J_\perp/J_z$, Eq. (15). We found that the effective Hamiltonian could be cast into a convenient form by performing a unitary transformation that rotates all down-pointing (minority) spins to up-pointing spins and also by introducing a connectivity matrix (whose elements are 1 for nearest-neighbor spins and 0 otherwise). The latter makes it possible to convert the sums over nearest-neighbor lattice sites to sums over the entire lattice [Eq. (23)]. These transformations cast the terms of the effective Hamiltonian coming from each order of perturbation theory into a form rather convenient for analysis. The resulting terms are expressed explicitly in terms of the Ising variables on the lattice sites, the spin s, and the connectivity matrix. These terms were studied order by order in perturbation theory. We found that diagrams representing these terms naturally fell into two categories: contractible and noncontractible. Contractible diagrams are those whose dependence on some of the Ising variables is eliminated by summing with respect to their site index over all lattice points. Thus, a function of N Ising variables can be reduced to a function of less than N Ising variables after this "contraction" process. The allowed contractions depend on the lattice geometry, the 3:1 constraint, and the Ising nature of the spin variables. We termed noncontractible those diagrams for which it is not possible to perform a contraction (equivalently, a reduction in the number of relevant Ising variables).

The central result of the analysis of contractible and noncontractible diagrams is that all terms in the constrained degenerate perturbation theory up to and including fifth order are constant *within the 3:1 manifold*. Individual terms are shown to be constant by first contracting the diagrams as much as possible and then noting that the value of the diagram is unchanged under permutation among site indices associated with the Ising variables. The latter statement implies that the value of the diagram is independent of spin configurations allowed in the 3:1 manifold and hence a constant. In a similar manner, most terms at sixth order are also shown to be constant. However, we also observe that, at sixth order, there appears a "single large loop" diagram, which cannot be contracted and also defies the permutation arguments mentioned above. In fact, this loop diagram brings about nonconstant contributions to the effective Hamiltonian in the 3:1 manifold. Therefore, this is the lowest-order term which lifts the degeneracy of the 3:1 manifold (at least for $s>1$). The nonconstant sixth-order term includes effective interactions among spins on each hexagonal plaquette of the pyrochlore lattice. Depending on the arrangement of minority sites, there are five distinct kinds of plaquettes that may appear and we label them 0,1…,4 (see Table I). Using the results of our degenerate perturbation theory, we evaluate the energy of each of these plaquettes as a function of α and s and correct a mistake in Ref. 9. The 3:1 condition constrains the allowed ratios of the various plaquettes in the lattice and allows us to express the total energy of the system (up to an overall constant), Eq. (60), in terms of only three energies [Eq. (62)].

As a check on the results immediately above and as a further test of the robustness of those results, we also performed a large-s expansion in the easy-axis limit. As with the full quantum theory, we expanded the harmonic spin-wave energy in powers of α up to the sixth order, applied the diagrammatic analysis above involving contractible and noncontractible diagrams, and studied the resulting energy of the nonconstant sixth-order terms. The result [Eq. (82)] agrees exactly with the $\mathcal{O}(s)$ term obtained from the quantum degenerate perturbation theory [Eq. (64)]. This satisfying consistency tells us that the large-s limit and small-α limit commute, and thus our analysis is likely well controlled.

In the final section of the paper, we used the results of the degenerate perturbation theory to determine the low-energy states on the plateau as a function of s. Our result that the first nonconstant diagonal term in perturbation theory comes at sixth order is independent of the spin value s. However, terms that allow plaquettes (such as type 1) to resonate occur at order $6s$, which can either be larger or smaller than 6 depending on s. In the strict easy-axis limit, therefore, for $s \geqslant 3/2$, the low-energy states are therefore determined only by a diagonal effective Hamiltonian, which can be analyzed classically. In the large but finite s limit, we are able to resolve the degeneracy of the zero-flux manifold found in the large-s analysis (extended from that of Hizi and Henley[26] to the XXZ model). We predict a trigonal$_7$ state (see Fig. 12) to

be the exact ground state in this easy-axis limit and for large s, and numerical analysis suggests that this is obtained for $s \geqslant 2$. For $s=3/2$, the lowest-energy configuration we have found in the Ising limit is a massively degenerate set of states (for example, the $\sqrt{3}\times\sqrt{3}$ states, see Fig. 15). For $s \leqslant 1$, and for $s=3/2$, 2, 5/2 extrapolated to the isotropic limit, we find that the off-diagonal term in the effective Hamiltonian becomes dominant, and we suggest several likely candidates for the ground states in these cases. This includes a possible U(1) spin-liquid state, which would be quite remarkable if realized.

B. Implications and future directions

First, let us comment briefly upon the relevance to the spinel chromites. For $HgCr_2O_4$, it is known that the temperature at which the plateau forms (≈ 7 K) is comparable to the highest temperature at which magnetic order is observed. The theoretical estimate of the magnitude of the couplings in the effective Hamiltonian due to quantum fluctuations for $s=3/2$ is $K \approx 0.25$ J (from Table II). A crude estimate based on the measured Curie-Weiss temperature in $HgCr_2O_4$ (Ref. 6) would predict an ordering temperature $\lesssim 1$ K. However, the observation of significant spin-lattice coupling[8] in $HgCr_2O_4$ would suggest that other mechanisms—i.e., physics outside the Heisenberg model—must be behind the plateau formation and the magnetic ordering. Indeed, a recent study of a simple model of spin-lattice coupling gives a reasonable explanation of the plateau and its order, predicting stabilization of the **R** state.[10] It would be quite interesting to see whether quantum fluctuations might, however, play a role in the other chromite spinels, e.g., $CdCr_2O_4$.

We now move away from the experiments on $HgCr_2O_4$, where the spin-lattice interactions are most likely more important than quantum fluctuations. Instead, we would like to address a basic question that may be in the mind of the reader. In the pure spin-s isotropic Heisenberg model (i.e., $J_\perp = J_z = J$), is there a plateau at half-magnetization? At $s=\infty$, i.e., the strict classical limit, the answer is no, and indeed the magnetization is a simple linear function of field in this case. In principle, this question can be addressed by the $1/s$ expansion.[36] However, to the order studied, the situation remains unclear: the leading-order spin-wave spectrum remains gapless even in a field. Higher-order calculations in $1/s$ are required to resolve this question via that approach. Within the *XXZ* model, for any amount of anisotropy ($\alpha < 1$), a plateau is expected even in the classical limit, so by continuity it is likely to persist at smaller s. However, the extrapolation to $\alpha=1$ is not clear. In Appendix A, we present some simple calculations aimed at addressing the plateau width. In particular, we show that the plateau narrows both from above and below upon perturbing away from the Ising limit, where it is maximal. The plateau edges are determined by the points at which the gap to excitations with nonzero S^z vanishes. Unfortunately, unlike the calculation of the splitting within the plateau states (the main focus of this paper), the energy difference *between* the plateau ground state and excited states with higher and/or lower S^z is nonvanishing already at quadratic and/or linear order in α. Hence, a high-order calculation of this gap becomes much more involved than those in the bulk of this paper, and an extrapolation to the isotropic limit is probably not reliable. The existence of a plateau in the isotropic limit is a subject worthy of study by other methods.

Next, we turn to future applications of the formalism developed here to other problems. From our exposition, it should be evident that our methods generalize rather straightforwardly to other models of quantum antiferromagnets with Ising anisotropy, provided a few conditions hold. First, the lattices should be composed of site-sharing simplexes. A simplex is a collection of sites in which every pair of sites is connected by a bond; examples include triangle, crossed square, and tetrahedron. Second, the ground states of the Ising part of the Hamiltonian on a single simplex should all be permutations of one another. This allows Ising exchange, single-site anisotropies, biquadratic, and other interactions. Third, the interactions should be the same on each bond but could include quite arbitrary combinations of exchange, biquadratic couplings, etc. There are quite a number of interesting models of frustrated magnetism which share these features. For instance, the *XXZ* models on the Kagome and checkerboard lattices can be studied this way at several values of the magnetization. The *XXZ* model on the pyrochlore lattice at zero field is also such a system. It will be interesting to explore the behavior of these models at various values of s using the methods of this paper.

More generally, the methods of this paper are possible because of a key simplification: in a strong magnetic field, the symmetry of the spin Hamiltonian is U(1) rather than SU(2). Many more theoretical methods are available to treat systems with *Abelian* conserved charges than for SU(2)-invariant spin models. Furthermore, in the interesting search for spin-liquid states of quantum antiferromagnets, much theoretical success has been achieved in recent years in realizing such states in U(1)-symmetric models, while examples of SU(2)-invariant spin liquids, even in models, are much more limited. Therefore, it seems likely that quantized magnetization plateaus may be an excellent hunting ground for such exotic states of matter, and, moreover, there is hope for theory and experiment to meet on this plane.

ACKNOWLEDGMENTS

This work was supported by NSF Grant No. DMR04-57440, PHY99-07949, and the Packard Foundation. R.S. acknowledges support from JSPS.

APPENDIX A: EDGES OF THE MAGNETIZATION PLATEAU

In this appendix, we analyze the gap to spin excitations above the 3:1 plateau. To lowest order in the transverse spin fluctuations, in the field range corresponding to the plateau in the Ising model, excitations carrying $\Delta S^z = \pm 1$ are separated by an energy gap of order J_z from the manifold of half-polarized states. As the magnetic field is varied, this gap decreases. At zero temperature, the magnetization plateau ends when the energy gap to one of these spinful excitations

vanishes. We shall consider the spin $\Delta S=\pm 1$ "single particle" excitations above the 3:1 manifold only and find a rough perturbative estimate for the limits of the half-magnetization plateau region. Clearly, the plateau region cannot extend beyond the magnetic-field values at which the gap to these excitations vanishes and so can only be more narrow than the extent we shall find here.

Consider $\Delta S=+1$ excitations above the ground state. These excitations are more favorable in higher magnetic fields. The simplest way to insert such an excitation is by raising one minority spin by one unit, i.e., obtained by acting with S_j^+ on a minority site to change $S_j^z=-s$ to $S_j^z=1-s$. This creates two "defective" tetrahedra (shared by this site), which no longer have the optimal 3:1 spin configuration. We will call the space of such states "manifold A." For $s>1/2$, manifold A comprises all the *lowest-energy* $\Delta S=+1$ excitations in the Ising Hamiltonian. Other $\Delta S=+1$ states, which involve more spin raising/lowering operators, e.g., those created by $S_i^+S_j^+S_k^-$, have higher energy because they either create more defect tetrahedra or make the two defect tetrahedra more energetically costly. The exception is $s=1/2$, for which manifold A is actually incomplete, and there are other $\Delta S=+1$ excitations outside it with the same zeroth-order energy. We will henceforth assume $s>1/2$ in the remainder of this appendix to avoid this complication.

The zeroth-order energy difference from the ground-state manifold is

$$E_A^0 - E_{3:1}^0 = 2J_z(3s-h). \tag{A1}$$

The gap shrinks as h increases and vanishes at a magnetic field $h_A=3s$. This corresponds to the high-field edge of the half-polarized plateau in the $\alpha=0$ limit. The single-site excitation is, however, highly degenerate. The excitation can reside on any of $N/4$ minority sites (N is the number of pyrochlore sites). We expect that breaking this massive degeneracy (i.e., having this magnon "flatband" acquire some dispersion) will lower the energy of this excitation (closing the gap at lower magnetic field). One therefore needs to take into account corrections from higher orders in DPT.

To first order in α, only spin $\Delta S_i^z=\pm 1$ can be transferred from one site to a nearest neighbor. In any 3:1 configuration, the nearest minority spins reside on next nearest neighboring sites *in the lattice sense*, which means that these sites are a distance of two *links* apart. Therefore, this process always leaves manifold A, and the first-order term has no contribution.

To second order in α, there are various viable processes. Apart from hopping spin 1 between neighboring sites and then back, there is also a nontrivial process in which the defect site (the $-s+1$ spin) swaps with one of the (next-) nearest-neighbor minority spins. This is also a legitimate member of the manifold A. Processes not involving the defect directly are affected by the presence of the defect only when involving the nearest neighbors of the defect site. All other sites have the same contribution to the second-order correction as in the ground-state manifold.

We immediately conclude that the form of the effective "magnon Hamiltonian" to second order is

$$\mathcal{H}_A^2 - \mathcal{H}_{3:1}^2 = -\left[c_1 + c_2 \sum_{\langle\langle ij\rangle\rangle} (e_i^\dagger e_j + \text{H.c.})\right], \tag{A2}$$

where $\langle\langle ij\rangle\rangle$ denotes next-nearest-neighbor sites on the pyrochlore lattice that are both minority sites, $c_{1,2}>0$ are coefficients depending on the physical couplings, and the operator $e_j^\dagger$ creates a local excitation—it replaces a spin $S_j^z=-s$ with a spin $S_j^z=1-s$ on site j:

$$e_j^\dagger = |-s\rangle_j\langle 1-s|_j. \tag{A3}$$

An arduous yet straightforward calculation for manifold A results in

$$\mathcal{H}_A^2 - \mathcal{H}_{3:1}^2 = -\frac{J_z\alpha^2}{2s-1}\left[\frac{3s(4s^2-3s+1)}{4s-1} + \frac{s^2}{2}\sum_{\langle\langle ij\rangle\rangle}(e_i^\dagger e_j + \text{H.c.})\right]. \tag{A4}$$

Note the singularity in Eq. (A4) for $s=1/2$, which reflects the incompleteness of manifold A in this case.

In a hopping Hamiltonian of the form of Eq. (A4), the magnon eigenstates are delocalized Bloch states. The spectrum of these states, in general, depends in detail upon the structure of the lattice of minority sites. However, if we are interested in the minimum energy state only, there is an amusing simplification. Since the hopping above is everywhere negative, the lowest-energy state is expected to be nodeless. Thus, the minimum energy state is simply a *constant amplitude* (i.e., zero quasimomentum) Bloch state. For any configuration of the minority spins $|\Psi_0\rangle$ in the ground-state manifold, the corresponding state in manifold A is

$$|\Psi\rangle = \sum_j e_j^\dagger|\Psi_0\rangle. \tag{A5}$$

Direct calculation yields

$$\sum_{\langle\langle ij\rangle\rangle}(e_i^\dagger e_j + \text{H.C.})|\Psi\rangle = 6|\Psi\rangle, \tag{A6}$$

where 6 comes about as the number of next-nearest neighbors with spin $S_j^z=-s$ the excitation can hop over to. Because in any 3:1 configuration there are always precisely six minority spins two links away, we are therefore able to obtain the lowest-energy $\Delta S^z=+1$ magnon energy *irrespective of the particular arrangement of the minority sites*.

The minimum energy of Eq. (A4) is therefore

$$E_{A,min}^2 - E_{3:1}^2 = -J_z\alpha^2\frac{3s(8s^2-4s+1)}{(2s-1)(4s-1)}. \tag{A7}$$

The combined gap to manifold A is now

$$\Delta E_A = J_z 2(3s-h) - J_z\alpha^2\frac{3s(8s^2-4s+1)}{(2s-1)(4s-1)}. \tag{A8}$$

The gap vanishes at a magnetic field of

$$h_A = 3s - \alpha^2\frac{3s(8s^2-4s+1)}{2(2s-1)(4s-1)}. \tag{A9}$$

Note that for $s\gg 1$, the $O(\alpha^2)$ correction is well behaved, i.e., it scales in the same way as the zeroth-order threshold field.

Excitations with $\Delta S=-1$ (manifold B) can be realized by replacing a spin $S_j^z=+s$ with a spin $S_j^z=s-1$. The zeroth-order energy difference from the ground-state manifold is calculated in an identical manner as in the $\Delta S=+1$ case and yields

$$E_B^0 - E_{3:1}^0 = 2J_z(h-s). \tag{A10}$$

At this order, the $\Delta S=\pm 1$ excitation spectra are symmetric about $h=2s$.

Oppositely from the behavior at the high-field edge of the plateau, the gap shrinks as h *decreases* and vanishes at a magnetic field $h_B=s$. Once again, due to a huge degeneracy (the defect can reside on any of $3N/4$ majority sites), we must resort to DPT in order to break the massive degeneracy of manifold B, expecting to lower the excitation energy.

In contrast to the $\Delta S^z=+1$ excitations above, it is already possible at first order to hop the spin $S^z=s-1$ onto other sites and stay within manifold B. This is because the majority sites are not isolated (four of the six neighboring sites of a majority site are also majority sites). Therefore, for any given 3:1 state, one can immediately obtain the effective Hamiltonian to $O(\alpha)$:

$$\mathcal{H}_B^1 = J_z s\alpha \sum_{ij} W_{ij} h_i^\dagger h_j. \tag{A11}$$

Here, W_{ij} is the connectivity matrix of the lattice of majority sites for the particular 3:1 state in consideration and the operator $h_j^\dagger$ creates a local excitation—it replaces a spin $S_j^z=s$ with spin $S_j^z=s-1$ on site j:

$$h_j^\dagger = |s-1\rangle_j \langle s|_j. \tag{A12}$$

Since $\alpha>0$, the hopping amplitudes in this case are positive, rather than negative as above. Thus, unfortunately, the lowest-energy eigenstate is a nontrivial Bloch state, whose energy depends upon the precise form of W_{ij}, i.e., it is different for each of the 3:1 states. Therefore, it is difficult to say anything specific about the $O(\alpha)$ correction to the minimum $\Delta S^z=-1$ magnon energy. Because one can easily construct variational states with negative hopping energy (e.g., an antibonding state with support only on two sites), the $O(\alpha)$ correction must be negative and, clearly from Eq. (A11), is of the form $E_B^1=-J_z s\alpha c$, with $c>0$ a dimensionless constant (the largest eigenvalue of W_{ij}). This gives

$$h_B = s(1+\alpha c) > s. \tag{A13}$$

Thus, the upper edge of the plateau decreases and the lower edge of the plateau increases as α is increased, narrowing the plateau with increasing quantum fluctuations. It is plausible that for sufficiently large α, the plateau is obliterated entirely, and the upper and lower edges meet. Unfortunately, this is beyond the realm of this perturbative analysis. Even a naïve extrapolation of the above lowest-order results is nontrivial, since the lower plateau edge depends upon the nontrivial constant c. It can, in principle, be computed for the various states obtained in Sec. V, but we do not do so here.

APPENDIX B: ALTERNATIVE CALCULATION OF THE DEGENERATE PERTURBATION THEORY

In this appendix, we present an alternative way of calculating the DPT sixth-order diagonal term, providing a check on the calculation described in Sec. III.

The perturbation (6) can be viewed as a sum over spin transfer operators,

$$\mathcal{H}_1 = \frac{\alpha}{2} J_z \sum_{\langle i,j\rangle} (\hat{S}_i^+ \hat{S}_j^- + \text{H.C.}) = \frac{\alpha}{2} J_z \sum_{\ell=\langle i,j\rangle} (\hat{h}_\ell + \text{H.C.}), \tag{B1}$$

where $\hat{h}_\ell$ transfers one quantum of spin angular momentum from site i to site j if this is on adjacent sites i,j. As a result, the nth order virtual processes can be classified by choosing n links to act on with spin transfer operators in a particular order. In order to return to the initial 3:1 configuration, the links must form closed loops of spin transfer. These include self-retracting loops, defined as loops where after following some path in the lattice, we turn back and travel the same path in the reverse order back to the origin. The chosen links can be represented by a graph on the lattice by coloring these links. Apart from the graph, we must also specify the order by which the links operate.

The virtual states in a DPT process will have a number of sites in a different spin state relative to the initial 3:1 state. We denote $S_j^z=\sigma_j(s-m_j)$, where the variables m_j are nonnegative and take on any integer value between 0 and $2s$. Let us denote the set of modified sites by M. Thus $m_j\neq 0$ only if $j\in M$. Using the fact that $\Sigma_j \sigma_i = \frac{1}{2}\Sigma_j 1$ and $\Sigma_{\langle ij\rangle}\sigma_i\sigma_j=0$, both due to the 3:1 constraint, we find that the inverse resolvent can be rewritten as a sum involving only the modified sites,

$$\begin{aligned}\mathcal{H}_0 - E_0 &= J_z \sum_{\langle ij\rangle} S_i^z S_j^z - E_0' = J_z \sum_{\langle ij\rangle} \sigma_i\sigma_j (s-m_i)(s-m_j) - E_0' \\ &= J_z \left(\sum_{\langle ij\rangle \in M} \sigma_i\sigma_j m_i m_j + 2s \sum_{j\in M} m_j \right) - E_0'',\end{aligned} \tag{B2}$$

where we have absorbed all constant energies into E_0''. With all $m_j=0$, this resulting energy should vanish (energy difference to a state in the 3:1 manifold) and therefore conclude that the energy $E_0''=0$ in the final expression above. Finally, our virtual state energy is

$$\mathcal{H}_0 - E_0 = J_z \left(\sum_{\langle ij\rangle \in M} \sigma_i\sigma_j m_i m_j + 2s \sum_{j\in M} m_j \right). \tag{B3}$$

At first order, the perturbation (6) takes any initial state out of the 3:1 manifold and therefore gives no contribution (equivalently, no loop can be closed with only one link).

In second order, we must act on the same link twice to undo the spin transfer and return to the 3:1 manifold. Therefore, all nonvanishing processes are confined to one tetrahedron. The same process can act on one of the links of this tetrahedron, *with the same resolvents for a given order of the link operators*. Therefore, by summing up these diagrams, we will get a function of the spins on this tetrahedron, which is invariant under any permutation of the four sites (the sum is represented in a diagrammatic way drawn in Fig. 17). Therefore, the 3:1 configuration on any single tetrahedron

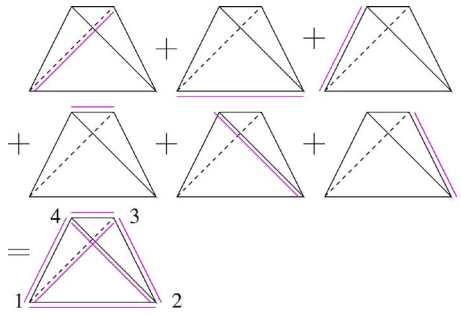

FIG. 17. (Color online) Second-order process.

has the same energy at this order in DPT, no matter which corner is chosen to be the minority site. For this reason, the second-order contribution gives a constant shift in energy to all the 3:1 states.

In third order, the only way one can return to the 3:1 manifold is by forming a single closed loop of spin transfer around a triangular side of a single tetrahedron. As in the second-order processes, we can sum over all such processes occurring on the single tetrahedron. One again, we end up with a function that is invariant under any permutation of the four sites of the single tetrahedron (the sum is represented in a diagrammatic way drawn in Fig. 18). Once again, we cannot distinguish energetically between the different 3:1 states defined on this single tetrahedron. As a result, the third-order term must produce a constant shift in energy.

As exemplified in the second- and third-order terms, all DPT processes (of any order) that are confined to one tetrahedron (meaning all the spin transfer operators act on links in the same tetrahedron) all add up to constant shifts in energy. In every such case, the argument is the same as above. Starting with a given process defined on a single tetrahedron, sum over all the processes of the *same structure* on the same tetrahedron. Then, one always arrives at a function that is invariant under any permutation of the four corners. Within the 3:1 manifold, these processes cannot favor one configuration over the other and must produce a mere shift in the overall energy. More explicitly, every process results in a function of the four Ising variables on a tetrahedron, as defined in Sec. II. The sum of all diagrams with the same structure then takes on the generic form

$$\begin{aligned} &f(\sigma_1,\sigma_2,\sigma_3,\sigma_4) + (\text{all permutations of } 1,\ldots,4) \\ &\quad = a_0 + a_1(\sigma_1+\sigma_2+\sigma_3+\sigma_4) \\ &\qquad + a_2(\sigma_1\sigma_2+\sigma_1\sigma_3+\sigma_1\sigma_4+\sigma_2\sigma_3+\sigma_2\sigma_4+\sigma_3\sigma_4) \\ &\qquad + a_3\sigma_1\sigma_2\sigma_3\sigma_4(\sigma_1+\sigma_2+\sigma_3+\sigma_4) + a_4\sigma_1\sigma_2\sigma_3\sigma_4. \end{aligned} \tag{B4}$$

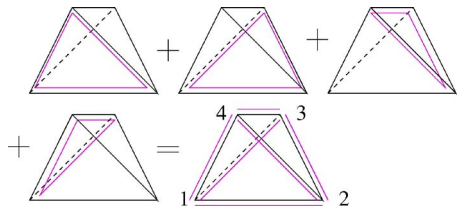

FIG. 18. (Color online) Third-order process.

The 3:1 constraint gives $\sigma_1\sigma_2\sigma_3\sigma_4=-1$ as well as $(\sigma_1+\sigma_2+\sigma_3+\sigma_4)=2$. The generic four spin function then reduces to

$$\begin{aligned} f(\sigma_1,\sigma_2,\sigma_3,\sigma_4) &= \text{const} + a_2\sum_{i<j=1}^{4}\sigma_i\sigma_j \\ &= \text{const} + \frac{a_2}{2}\left(\sum_{j=1}^{4}\sigma_j\right)^2 = \text{const}. \end{aligned} \tag{B5}$$

Given this result, we can always ignore virtual processes confined to one tetrahedron for the remainder of our discussion.

Similar arguments can be applied to processes confined to two adjacent tetrahedra. Summing over all possible processes confined to pairs of adjacent tetrahedra, one always ends up with a constant energy shift in the 3:1 manifold. A pair of adjacent tetrahedra can only be in one of three configurations in the 3:1 manifold (see Fig. 3). The adjacent tetrahedron pairs can be enumerated by the site connecting them. Therefore, the number of distinct pairs is equal to the number of pyrochlore sites. In the 3:1 manifold, the number of configurations where the shared site is a minority site [see Fig. 3(a)] is *fixed* to be $\frac{1}{4}$ of the sites. In the remaining $\frac{3}{4}$ of the sites, the shared site is a majority site. The two configurations in Fig. 3(a) with a majority site connecting the pair of tetrahedra are distinguishable physically because of the different directions of the links, but in terms of the diagrams defining DPT processes, Figs. 3(b) and 3(c) are *indistinguishable* (they are identical in the graph sense—the link structure is the same). Therefore, the summation over all possible processes confined to these two adjacent tetrahedra always results in a function of the Ising variable defined on the shared site,

$$f(\sigma_i) = a_0 + a_1\sigma_i. \tag{B6}$$

For each pair of adjacent tetrahedra, we have the same function (B6) of the shared site Ising variable. Summing over all pairs of adjacent tetrahedra is equivalent to summing over the sites of the pyrochlore lattice. Therefore, the sum of all the DPT processes of this sort results in

$$\sum_i f(\sigma_i) = Na_0 + a_1\sum_i \sigma_i = Na_0 + \frac{N}{2}a_1, \tag{B7}$$

where N denotes the total number of pyrochlore lattice points. Once again, we are led to the conclusion that all such processes can only give a constant shift in energy, and we shall ignore all such instances in the remainder of our discussion.

At fourth order, we have a number of possible processes. The only spin transfer processes comprising a single loop will be confined to two adjacent tetrahedra. According to the arguments above, this single loop process will give a constant shift in energy within the 3:1 manifold. Apart from single closed loop, we can only also have processes with two separate closed loops, comprising two nonoverlapping links which get acted on twice. Each chosen link occupies its own tetrahedron (if the two links are on the same tetrahedron, one must act on a bond with two majority spins, and automati-

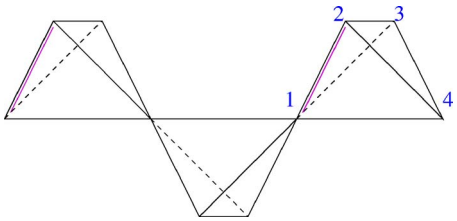

FIG. 19. (Color online) Fourth-order process.

cally produces zero). The case in which these two tetrahedra are adjacent will result in a constant, by our arguments above. Otherwise, there are only two possibilities. In one case, these two tetrahedra share a neighboring tetrahedron. In the second case, they are separated by more than one tetrahedra. This classification is necessary because, in the former case, different resolvents may show up through the interaction term of the virtual state energy (B3). If the two links are separated by more than one tetrahedron, this does not occur.

In the case where the two tetrahedra are sufficiently well separated, with no mutual interaction in the virtual state energy, we can once again invoke the trick of summing over all such processes on each single tetrahedron containing a link, and the DPT term cannot distinguish between the four 3:1 configurations on each tetrahedron. Once again, we end up with a constant shift in the overall energy for all the 3:1 configurations.

Now, we consider the processes where the two tetrahedra share a neighboring tetrahedron. One such diagram is pictured in Fig. 19. The structure spans a chain of three tetrahedra. In the present case, when summing over diagrams, one must be cautious to sum over diagrams with the same resolvents. Summing over equivalent diagrams on the chain of three tetrahedra, such as those found by permuting site 2 with 3 and 4, yields a function that treats the three sites at the outer side of each edge tetrahedron on equal footing. We graphically indicate the sum of diagrams by coloring all the links that appeared in one of the diagrams we summed over (see Fig. 20).

Formally, the sum of processes gives rise to a function of the eight Ising variables on the two edge tetrahedra $\tilde{f}(\sigma_1,\ldots,\sigma_8)$. Because of the above arguments, this function has to be invariant under permutations of the three outer edge spins. Considering all possible expressions we can form out of the three edge spins in a "symmetric" way,

$$f(\sigma_1,\ldots,\sigma_8) = a_0 + a_1(\sigma_2+\sigma_3+\sigma_4) + a_2(\sigma_2\sigma_3+\sigma_2\sigma_4+\sigma_3\sigma_4) + a_3\sigma_2\sigma_3\sigma_4, \tag{B8}$$

where the dependences of $a_{0,1,2,3}$ on $\sigma_{1,5,6,7,8}$ are implicit.

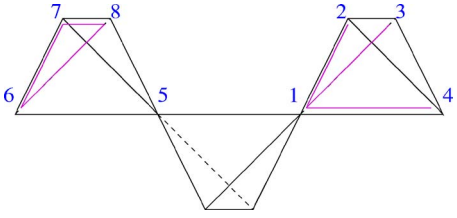

FIG. 20. (Color online) Sum of fourth-order processes.

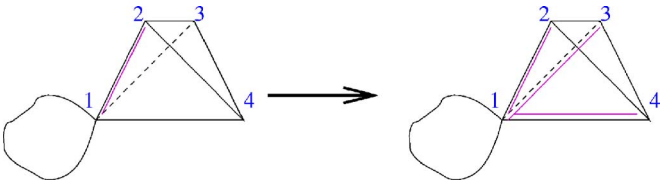

FIG. 21. (Color online) Summing over equivalent edges of a diagram to contract the dependence on sites in the cluster.

Using the 3:1 constraint on this tetrahedron $(\sigma_1+\sigma_2+\sigma_3+\sigma_4)=2$, as well as the identities it implies, $\sigma_1\sigma_2\sigma_3\sigma_4=-1$ (or $\sigma_2\sigma_3\sigma_4=-\sigma_1$) and $(\sigma_2\sigma_3+\sigma_2\sigma_4+\sigma_3\sigma_4)=1-2\sigma_1$, we find that $f(\sigma_1,\ldots,\sigma_8)$ can be rewritten as a function of $\sigma_{1,5,6,7,8}$ alone,

$$f(\sigma_1,\ldots,\sigma_8) = a_0 + a_1(2-\sigma_1) + a_2(1-2\sigma_1) - a_3\sigma_1 = \tilde{a}_0 + \tilde{a}_1\sigma_1. \tag{B9}$$

Repeating the same simplification for the three Ising variables of the other edge, $\sigma_{6,7,8}$, one finds that the sum of diagrams above can only produce a function depending on the two spins connecting the edge tetrahedra to the third tetrahedron in the middle of the chain (sites 1 and 5 in Fig. 20). This function is, therefore, a function of two neighboring spins on a single tetrahedron $\tilde{f}(\sigma_1,\sigma_5)$. Each three tetrahedron chain process can be represented by the pyrochlore link between the two sites shared between the tetrahedra (sites 1 and 5 in Fig. 20). Summing over all the processes represented by the six links in the central tetrahedron, which contains sites 1 and 5, one ends up with a function which is symmetric under a permutation of the four sites on this tetrahedron. Repeating the steps outlined in Eqs. (B4) and (B5), we find that the resulting function is constant.

The particular case analyzed above is only an example of a vastly more general case, which we now describe. Given a set of diagrams that reside on chains of tetrahedra, with the two edge tetrahedra not sharing a neighboring tetrahedron between them in any of the diagrams (except through the chain itself), one can sum over sites at the edge that we are free to permute (see examples in Figs. 21 and 22). The summation in both examples will result in a function of the spins at site 1. This procedure of *contracting* the diagram can be continued from both edges, and we will always end up with a function of two sites residing on one tetrahedron. We then sum over all the different choices of the last two remaining sites on this tetrahedron. We then end up with a symmetric function of the four sites on a single tetrahedron, which is always a constant, from Eqs. (B4) and (B5). Therefore, we

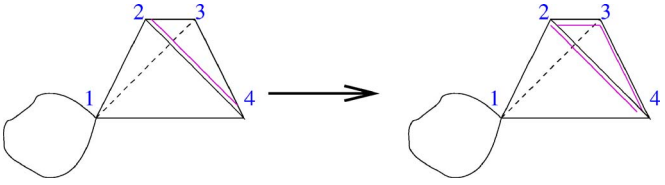

FIG. 22. (Color online) Summing over equivalent edges of a diagram to contract the dependence on sites in the cluster.

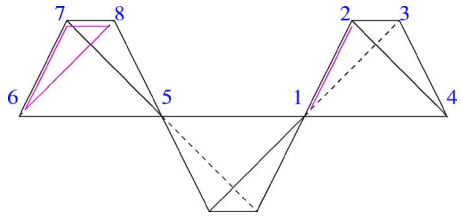

FIG. 23. (Color online) Fifth-order process.

conclude that all such diagrams can be summed over to give constant shifts in energy. We shall refer to these sets of diagrams as "retractable chains."

Bearing the above arguments in mind, we now turn to fifth order in DPT. Any diagram which consists of only one closed loop of spin transfer is confined to two adjacent tetrahedra. As elaborated above, the different 3:1 configurations on the pair of adjacent tetrahedra are indistinguishable in the graph sense. These diagrams can therefore contribute only a constant shift in energy. Other than these diagrams, the only possibility is to have two separate closed loops of spin transfer. One must involve a single link being acted on twice, and the other must be a three-link loop. Both loops reside on two different tetrahedra. If the two tetrahedra are adjacent, or share a neighboring tetrahedron (as in Fig. 23), the tetrahedra are part of a retractable chain. Our general analysis for retractable chains then applies here as well. Therefore, these diagrams must also sum up to a constant in the 3:1 manifold. Otherwise, the two tetrahedra are sufficiently well separated, and we can sum over the various diagrams on each tetrahedron separately. The summation gives an expression in which each of the four tetrahedron corners are on equal footing and cannot distinguish between different 3:1 states, resulting in a constant energy shift.

In agreement with the results of Sec. II, DPT terms of order less than 6 will not split the energy of the 3:1 states. Finally, we turn to sixth order in DPT,

$$\mathcal{H}_6 = -\mathcal{P}(\mathcal{H}_1\mathcal{R})^5\mathcal{H}_1\mathcal{P}, \tag{B10}$$

where $\mathcal{R}=(1-\mathcal{P})/(\mathcal{H}_0-E)$ is the resolvent. At this order, we have another new class of single closed loops—loops around hexagonal plaquettes of the pyrochlore lattice (see Fig. 24),

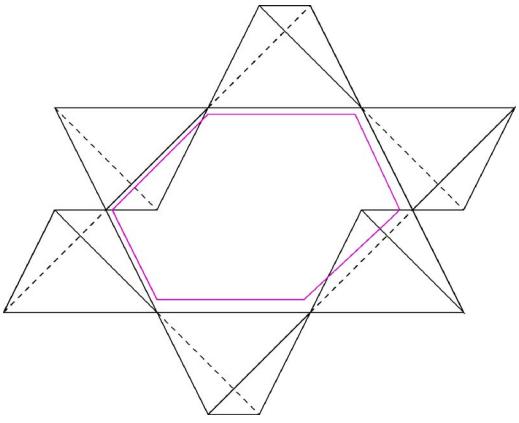

FIG. 24. (Color online) Hexagonal plaquette loop process.

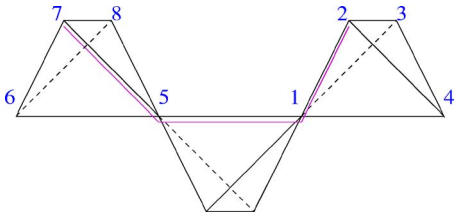

FIG. 25. (Color online) Single self-retracting loop on a chain of three tetrahedra.

which will split the energy of different 3:1 configurations. These processes can be enumerated by the hexagonal plaquettes they act on. So, we can write the contribution from these processes $\Sigma_{\mathcal{P}}\tilde{g}(\sigma_1,\ldots,\sigma_6)$ where the spins around the hexagonal plaquette are denoted by 1,…,6.

All other single closed-loop diagrams are confined to one, two, or three adjacent tetrahedra; the first two we already know will sum up to constant shifts in energy. The self-retracting loop residing on a chain of three tetrahedra is depicted in Fig. 25 and is also summed over to produce a constant, since this is a retractable chain.

Next, we consider the diagrams which comprise two closed loops. There must be two of length 3, or one of length 4, and one of length 2. In the case of two loops of length 3, each loop must reside on a single tetrahedron. If the two tetrahedra are adjacent, or even share a neighboring tetrahedron (as in Fig. 26), they form a retractable chain and result in a constant. Otherwise, the tetrahedra are sufficiently well separated so that we can sum over diagrams on the two tetrahedra separately and end up with a constant.

We now turn our attention to the case of one loop of length 4 and one of length 2. The loop of length 2 must be one link appearing twice and is therefore confined to a single tetrahedron. The loop of length 4 must be confined to two adjacent tetrahedra (or even just 1). If the two loops are sufficiently well separated (by more than one tetrahedra), we can sum over all two-loop diagrams in the tetrahedron, where the loop of length 2 resides, resulting in a constant. We can then sum over diagrams on the tetrahedron cluster containing the four loops to produce another constant. If the two clusters are adjacent, or separated by just one tetrahedron, we have a retractable chain, which we have already shown must result in a constant.

The last set of sixth-order diagrams is that of three closed loops, each comprising a single link, acted on twice. Each loop is therefore confined to a single tetrahedron. Using the same arguments as before, if all three tetrahedra are separated by more than one tetrahedron from one another, we can

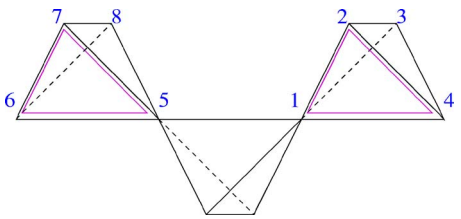

FIG. 26. (Color online) Sixth-order diagram with two loops of length 3.

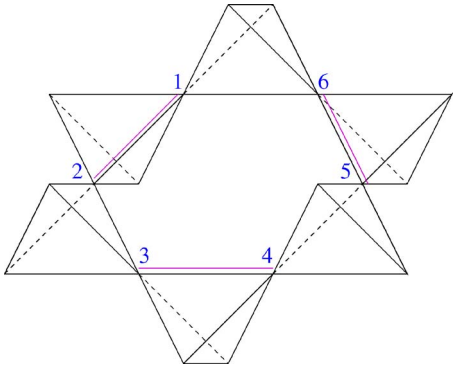

FIG. 27. (Color online) Three-loop diagram residing on a closed chain of tetrahedra, enclosing a hexagonal plaquette. This is the "f" process.

sum over all such diagrams contained in the same tetrahedra. In particular, sum over diagrams related by permuting over sites on each single tetrahedron separately results in a constant. Even if only one tetrahedron is well separated from the other two, we can first sum over diagrams on the isolated tetrahedron to produce a constant and then deal with the other two tetrahedra. The remaining two will reside on a retractable chain of tetrahedra, again resulting in a constant.

The only cases which we must deal with more carefully are those diagrams where each pair of tetrahedra either shares a neighboring tetrahedron or the two are adjacent. When at least one pair of loops resides on adjacent tetrahedra, the cluster of tetrahedra will always be a retractable chain, with either four or three tetrahedra. We are left only with diagrams where all three tetrahedra containing the loops are not adjacent but rather have shared neighboring tetrahedra. There are three tetrahedron clusters possible where this occurs. Figure 27 shows a diagram residing on a closed chain of six tetrahedra, enclosing a hexagonal plaquette. This is not a retractable chain. In Fig. 28, the three tetrahedral containing the loops all share one single neighboring tetrahedron. Finally, in Fig. 29, the three loops reside on a linear chain of five tetrahedra. However, it is important to note at this point that the tetrahedra at the two edges of this chain (1 and 7) can be identified to give the cluster shown in Fig. 27.

The processes on the cluster shown in Fig. 27 cannot be contracted and will split the energy of the different 3:1 states. We denote the sum of processes with the three loops on the same tetrahedra as in Fig. 27, $f(\sigma_1,\ldots,\sigma_6)$. There is also a

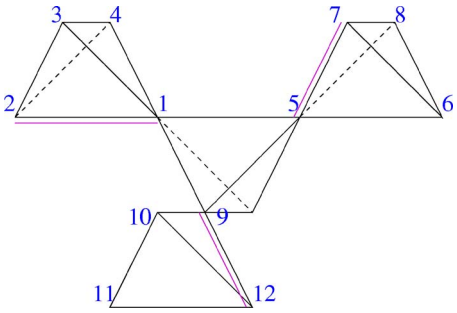

FIG. 28. (Color online) Diagram contributing to the function "g."

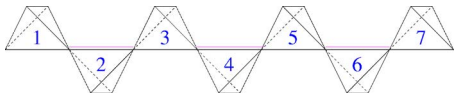

FIG. 29. (Color online) Diagram contributing to the function "r." The loops are embedded in the tetrahedra marked 2, 4, and 6.

contribution from all the processes where the three loops reside on the complementary set of tetrahedra, which must result in $f(\sigma_6,\sigma_1\ldots\sigma_5)$ (the same function with the spins cyclically permuted once). Cyclically permuting the spins again takes us back to the set of processes we summed over in $f(\sigma_1,\ldots,\sigma_6)$, and therefore f must be invariant under two permutations. This is a good check for the correctness of the result we find. The sum $f(\sigma_1,\ldots,\sigma_6)+f(\sigma_6,\sigma_1,\ldots,\sigma_5)$ accounts for all the diagrams on a given cluster enclosing a plaquette, and the total contribution to the effective Hamiltonian can be written as

$$\sum_{\mathcal{P}} [f(\sigma_1,\ldots,\sigma_6)+f(\sigma_6,\sigma_1,\ldots,\sigma_5)]. \tag{B11}$$

The processes on the cluster shown in Fig. 28 can be contracted from the "loose ends" of the diagram, similar to the contraction we have implemented for the retractable chains. For the particular example in Fig. 28, we sum over the corresponding diagrams with 2 permuted with 3 and 4. The resulting sum can only be a function of sites 1, 5, 7, 9, and 12. We then sum over the corresponding diagrams with 7 permuted with 6 and 8 and then sum over 12 permuted with 10 and 11. After these summations, the resulting function can only be a function of the sites 1, 5, and 9. Finally, we sum over all choices of three such sites on the central tetrahedron, which must result in a constant (a symmetric function of the four sites of a single tetrahedron).

Next, we turn to the processes on the chain in Fig. 29. At first glance, it would seem that these are retractable diagrams that will amount to a constant. Such a summation would include 81 different diagrams (we retract the tetrahedra 2, 3, 5, and 6, each time summing over three permutations of sites). However, two of these diagrams are of the form of Fig. 27, in which case the tetrahedra 1 and 7 at the edges of the chain are *identified*. As a result, these two diagrams may have *different* resolvents from the other 79 diagrams in this sum, since the sites on tetrahedra 1 and 6 may now interact. These two terms have, in fact, already been taken into account in $f(\sigma_1,\ldots,\sigma_6)$ and therefore should not be added again to the effective Hamiltonian. The summation that makes contractible diagrams give constant energy shifts requires that the resolvents be *identical* for the entire set of diagrams.

Rather than explicitly calculating the remaining 79 diagrams, we employ the following trick. In order to produce a constant, we add to the 79 diagrams two terms having the same resolvent, but replacing the spin variables σ_j with those at the positions 1–6 in Fig. 27. All these 81 terms have the same resolvent as that of the process in Fig. 29 and therefore will result in a constant. The two additional terms *do not* represent actual DPT processes and therefore must be subtracted from the effective Hamiltonian. The terms we need to

subtract are enumerated by the choice of central tetrahedron in the chain in Fig. 29 (tetrahedron 4), which we can identify with the tetrahedron containing sites 3 and 4 in Fig. 27. Given a choice of the central tetrahedron, each term of this sort is a function of the six spins $r(\sigma_1, \ldots, \sigma_6)$ as defined in Fig. 27. Given a hexagonal plaquette, there are six choices of the central tetrahedron and, correspondingly, six terms, and we must take all of these into account. Choosing a different central tetrahedron is equivalent to cyclically permuting the spins 1,…,6, and so the total contribution of all these processes is

$$-\sum_{\mathcal{P}} [r(\sigma_1, \ldots, \sigma_6) + r(\sigma_6, \ldots, \sigma_5) + r(\sigma_5, \ldots, \sigma_4) + r(\sigma_4, \ldots, \sigma_3) + r(\sigma_3, \ldots, \sigma_2) + r(\sigma_2, \ldots, \sigma_1)]. \quad \text{(B12)}$$

The sixth-order term in the effective Hamiltonian finally reads

$$\mathcal{H}_6 = \sum_{\mathcal{P}} g(\sigma_1, \ldots, \sigma_6) + \sum_{\mathcal{P}} [f(\sigma_1, \ldots, \sigma_6) + f(\sigma_6, \sigma_1, \ldots, \sigma_5)] - \sum_{\mathcal{P}} [r(\sigma_1, \ldots, \sigma_6) + r(\sigma_6, \ldots, \sigma_5) + r(\sigma_5, \ldots, \sigma_4) + r(\sigma_4, \ldots, \sigma_3) + r(\sigma_3, \ldots, \sigma_2) + r(\sigma_2, \ldots, \sigma_1)]. \quad \text{(B13)}$$

Calculating these functions explicitly, we find the *exact* same results as in Sec. II.

APPENDIX C: SPIN $s=\frac{3}{2}$ DIAGONAL TERM GROUND-STATE DEGENERACY

In this appendix, we analyze the lowest-energy states found for the diagonal term in the effective Hamiltonian for spin $s=\frac{3}{2}$ discussed briefly in Sec. V A 4. The lowest-energy states turn out to be massively degenerate. We have found what is at the very least a subset of this manifold, which already exhibits a degeneracy that grows with the system size, diverging in the thermodynamic limit.

First, we consider all the possible states we can construct with all the Kagome layers in the pyrochlore taking on the $\sqrt{3}\times\sqrt{3}$ configuration in Fig. 15. Given a plane in this $\sqrt{3}\times\sqrt{3}$ configuration, there are three different ways to place the following layer (also in the $\sqrt{3}\times\sqrt{3}$ configuration) above it, as described in Fig. 30. This freedom in the way the planar configurations are stacked is the source of a massive degeneracy—there are 3^L possible stacking choices, where L is the linear dimension in the $\langle 111\rangle$ direction of the system. Also, there are four plaquette directions in which to choose the direction of the stacking, resulting in an overall number of such states 4×3^L. For now, we shall work with this subset of the entire degenerate manifold, since these states are rather easy to handle. We shall refer to this set of states as the $\sqrt{3}\times\sqrt{3}$ states.

Now, we turn to calculate the energy of these states, proving that these are degenerate states. Each plaquette in the $\sqrt{3}\times\sqrt{3}$ planes shares links with three plaquettes above it. These four plaquettes enclose an up-headed cell, as defined

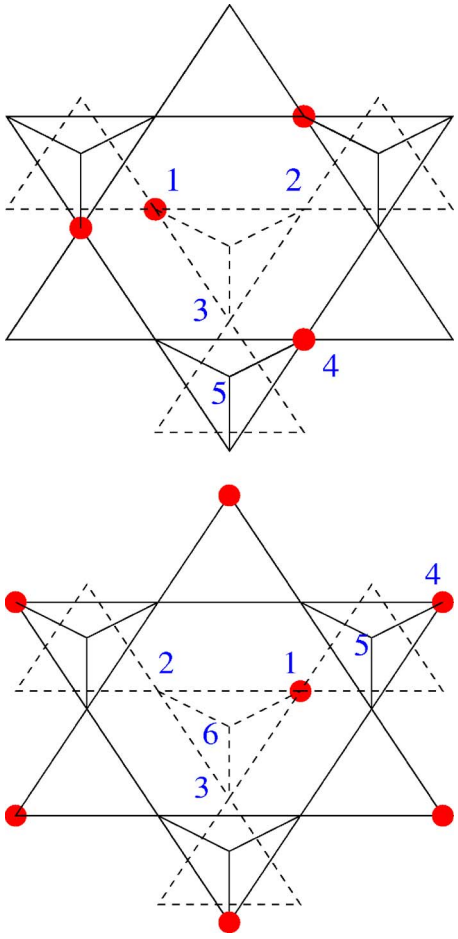

FIG. 30. (Color online) Stacking of two planar $\sqrt{3}\times\sqrt{3}$ states. The solid lines represent the tetrahedra of the lower plane. The dashed lines represent the tetrahedra of the upper layer. The same convention regarding up-pointing and down-pointing tetrahedra applies here as in Fig. 12 for both the solid and dashed line triangles. In both figures, the dashed tetrahedron with the corners 1, 2, and 3 must have one of these three corners a minority site [marked by solid (red) circles], and any of these three can be chosen. Once the minority site has been chosen from 1, 2, and 3, the $\sqrt{3}\times\sqrt{3}$ state of the upper layer is then uniquely determined. The choice of site 1 is explicitly shown in both cases.

in Sec. V A. For any of the $3\sqrt{3}\times\sqrt{3}$ spin configurations of the next Kagome plane, we always get the same up-headed cell types above the type 1 and type 0 plaquettes in the $\sqrt{3}\times\sqrt{3}$ plane. The clusters enclosing these up-headed cells above the type 1 and type 0 plaquettes are depicted in Figs. 30(a) and 30(b), respectively. Since we are only considering up-headed cells, every one of the plaquettes appears in only one cell.

Inspection of Fig. 30(a) shows that it includes one plaquette of type 1, one of type 2, one of type 3, and one of type 4 (this is just the type 1 cell in Table III). For the cluster in Fig. 30(b), we find that it includes two type 0 plaquettes, and two type 2 (type 8 cell in Table III). Of the plaquettes in the planes, which comprise $\frac{1}{4}$ of the plaquettes in the lattice, $\frac{2}{3}$ are in a type 1 configuration and $\frac{1}{3}$ are in a type 0 configuration. Since each planar plaquette determines the configura-

tion of the unique up-headed cell it is a part of, we therefore find that $\frac{2}{3}$ of the up-headed cells are type 1 cells $\left(y_1=\frac{2}{3}\right)$ and the remaining $\frac{1}{3}$ are type 8 cells $\left(y_8=\frac{1}{3}\right)$. The corresponding plaquette-type fractions are $x_0=\frac{1}{6}$, $x_1=\frac{1}{6}$, $x_2=\frac{1}{3}$, $x_3=\frac{1}{6}$, and $x_4=\frac{1}{6}$. Finally, the energy per plaquette of the $\sqrt{3}\times\sqrt{3}$ states is

$$\frac{1}{N}E_{\sqrt{3}\times\sqrt{3}}=\frac{1}{6}(V_1+2V_2+V_4). \tag{C1}$$

We expect the fractions of plaquettes in all the states in this degenerate manifold to be the same as in this subset, since, otherwise, it is rather unlikely (though not impossible) that a different combination of fractions will yield the same energy.

Having analyzed this set of states we turn to an additional set of states, with the same energy. Consider a particular subset of $\sqrt{3}\times\sqrt{3}$ states, with every two Kagome planes stacked in the same manner. This subset of the $\sqrt{3}\times\sqrt{3}$ states has a total of $4\times3^2=36$ states—factor of 4 for choosing the direction of the layering, a factor of 3 for the choice of how to position the planar configuration on one plane, and another factor of 3 from the freedom to choose how to stack the next planar layer. We shall refer to these as the uniformly stacked states.

Starting from any of these uniformly stacked states, we note that the type 1 cell can swap its type 1 and 3 plaquettes by changing the position of only one minority site. In Fig. 30(a), this can be accomplished by moving the minority site at site 4 to site 5. In addition, site 5 is part of a type 8 cell, and it is denoted also in Fig. 30(b), where it is evident that in order to maintain the 3:1 constraint, we must also shift the minority site at site 1 in Fig. 30(b) to site 6. Because the stacking of the next layer is *exactly* the same, the same shifting of minority sites must occur along the entire straight line passing through site 4 in the direction from site 4 to site 5. Closing this chain at infinity makes this chain into an infinite length loop of alternating minority and majority sites that are *flipped*, and, therefore, this maintains the 3:1 constraint. One can convince oneself from Fig. 30(b) that the type 8 cell will remain a type 8 cell under these minority site shifts. Since all the cells remain in the same configuration type, the plaquette-type fractions remain the same as in the $\sqrt{3}\times\sqrt{3}$ states, have the same energy, and are therefore degenerate.

We now turn to calculate the degeneracy of this set of states. Each type 8 cell has exactly one site it can shift in this manner, but since the chains are not shared between different type 0 plaquettes in the plane, one can convince oneself that these straight line chains of sites can be flipped *independently*. Therefore, starting from a particular uniformly stacked state, since there are $N/4L$ plaquettes in every plane (where N is the number of pyrochlore sites and the number of hexagonal plaquettes), there are $N/12L$ chains we can independently flip between two configurations, resulting in a degeneracy of $36\times2^{N/12L}$. However, an additional subtlety must be addressed.

Every $\sqrt{3}\times\sqrt{3}$ state has all the up-pointing tetrahedra in one of three 3:1 configurations. Flipping any chain in a uniformly stacked state will introduce some number of up-pointing tetrahedra in the fourth possible 3:1 configuration of a single tetrahedron. Starting from one uniformly stacked state, flipping all possible chains, we will change all the tetrahedra of one of the three 3:1 configurations into the fourth tetrahedron configuration type, which was absent in the initial uniformly stacked state. Once again, we will find ourselves with all tetrahedra in only three possible different 3:1 configurations. This suggests that perhaps this final state we have reached is also a uniformly stacked state. From inspection, we find that this indeed is the case, so that from one uniformly stacked state we can reach one other such state by flipping all possible chains in the manner described above. We must therefore correct the degeneracy to $18\times2^{N/(12L)}$ to account for this double counting.

In total, we have found the degeneracy of these two sets of states to be

$$18\times2^{N/12L}+4\times3^{L}-36, \tag{C2}$$

where we have subtracted 36 since this is the number of states that appear in both sets of states we have analyzed (these are simply the uniformly stacked states). We shall refer to the combined set of states as the 1-8 manifold of states, since it involves only type 1 and type 8 cells. The degeneracy we have calculated matches *precisely* the degeneracies in Table V for all the clusters where we have found the lowest-energy state for $s=\frac{3}{2}$, namely, the $3\times3\times1$, $6\times3\times1$, $3\times3\times2$, and $3\times3\times3$ clusters. Our analysis clearly shows that this set of states is massively degenerate, and despite exhausting all the states we have found numerically with this energy, we cannot be certain that these exhaust all possible states with this energy.

In a previous publication,[10] analyzing the same 3:1 degenerate manifold of states, the authors ascertained the maximum fraction of type 1 plaquettes that can be placed on a pyrochlore lattice is $\frac{1}{4}$. The 1-8 states do not realize this limit but come fairly close to it with $\frac{1}{6}$ of the plaquettes in the type 1 configuration. Therefore, the $\sqrt{3}\times\sqrt{3}$ states are a "compromise" between the energy gain of V_1 (which favors the type 1 plaquettes) and the energy loss of V_2 (which disfavors the type 2 plaquettes), taking into account the constraint $x_1<x_2$. This becomes evident when calculating the energy of the various cell types. The state realizing the maximum fraction of type 1 plaquettes found in Ref. 10 comprised only type 2 cells. For $s=\frac{3}{2}$, type 1 cells are far more favorable in energy than type 2 cells, and type 1 cells are abundant in the 1-8 states.

[1] P. Fazekas and P. W. Anderson, Philos. Mag. **30**, 423 (1974).
[2] M. Hermele, M. P. A. Fisher, and L. Balents, Phys. Rev. B **69**, 064404 (2004).
[3] J. Alicea, O. I. Motrunich, and M. P. A. Fisher, Phys. Rev. Lett. **95**, 247203 (2005).
[4] R. Moessner, S. L. Sondhi, and P. Chandra, Phys. Rev. B **64**, 144416 (2001).
[5] S. Sachdev, Phys. Rev. B **45**, 12377 (1992).
[6] H. Ueda, H. Mitamura, T. Goto, and Y. Ueda, Phys. Rev. B **73**, 094415 (2006).
[7] H. Ueda, H. A. Katori, H. Mitamura, T. Goto, and H. Takagi, Phys. Rev. Lett. **94**, 047202 (2005).
[8] M. Matsuda *et al.* (unpublished).
[9] D. L. Bergman, R. Shindou, G. A. Fiete, and L. Balents, Phys. Rev. Lett. **96**, 097207 (2006).
[10] D. L. Bergman, R. Shindou, G. A. Fiete, and L. Balents, cond-mat/0605467 (unpublished).
[11] K. Penc, N. Shannon, and H. Shiba, Phys. Rev. Lett. **93**, 197203 (2004).
[12] Y. Motome, K. Penc, and N. Shannon, J. Magn. Magn. Mater. **300**, 57 (2006).
[13] N. Shannon, K. Penc, and Y. Motome, cond-mat/0510333 (unpublished).
[14] G. W. Chern, C. J. Fennie, and O. Tchernyshyov, cond-mat/0606039 (unpublished).
[15] V. R. Chandra, S. Ramasesha, and D. Sen, Phys. Rev. B **70**, 144404 (2004).
[16] Y. Narumi, K. Katsumata, Z. Honda, J. C. Domenge, P. Sindzingre, C. Lhuillier, Y. Shimaoka, T. C. Kobayashi, and K. Kindo, Europhys. Lett. **65**, 705 (2004).
[17] M. Matsumoto, Phys. Rev. B **68**, 180403(R) (2003).
[18] H. Tanaka, T. Ono, H. A. Katori, H. Mitamura, F. Ishikawa, and T. Goto, Prog. Theor. Phys. Suppl. **145**, 101 (2002).
[19] S. Miyahara, F. Becca, and F. Mila, Phys. Rev. B **68**, 024401 (2003).
[20] G. Misguich, T. Jolicoeur, and S. M. Girvin, Phys. Rev. Lett. **87**, 097203 (2001).
[21] M. Uchida, H. Tanaka, M. Bartashevich, and T. Goto, J. Phys. Soc. Jpn. **70**, 1790 (2001).
[22] T. Momoi and K. Totsuka, Phys. Rev. B **62**, 15067 (2000).
[23] O. Starykh (unpublished).
[24] W. Zheng, J. O. Fjaerestad, R. R. P. Singh, R. H. McKenzie, and R. Coldea, Phys. Rev. Lett. **96**, 057201 (2006).
[25] J. von Delft and C. L. Henley, Phys. Rev. B **48**, 965 (1993).
[26] U. Hizi and C. L. Henley, Phys. Rev. B **73**, 054403 (2006).
[27] C. L. Henley, Phys. Rev. Lett. **96**, 047201 (2006).
[28] D. S. Rokhsar and S. A. Kivelson, Phys. Rev. Lett. **61**, 2376 (1988).
[29] R. Moessner and S. L. Sondhi, Phys. Rev. Lett. **86**, 1881 (2001).
[30] D. A. Huse, W. Krauth, R. Moessner, and S. L. Sondhi, Phys. Rev. Lett. **91**, 167004 (2003).
[31] O. F. Syljuasen, cond-mat/0512579 (unpublished).
[32] K. Damle and T. Senthil, cond-mat/0602671 (unpublished).
[33] D. L. Bergman, G. A. Fiete, and L. Balents, Phys. Rev. B **73**, 134402 (2006).
[34] L. Pauling, J. Am. Chem. Soc. **57**, 2680 (1935).
[35] S. T. Bramwell and M. J. P. Gingras, Science **294**, 1495 (2001).
[36] S. R. Hassan and R. Moessner, Phys. Rev. B **73**, 094443 (2006).